Low Frequency Electromagnetic Fields in High Contrast Media *

Liliana Borcea[1] and George C. Papanicolaou[2]

[1] Computational and Applied Mathematics, MS 134, Rice University, 6100 Main Street, Houston, TX 77005-1892 borcea@caam.rice.edu
[2] Department of Mathematics, Stanford University, Stanford, CA 94305 papanicolaou@stanford.edu

Abstract. Using variational principles we construct discrete network approximations for the Dirichlet to Neumann or Neumann to Dirichlet maps of high contrast, low frequency electromagnetic media.

1 Introduction

Imaging of the electrical conductivity and permittivity of a heterogeneous body by means of low-frequency electrical or electromagnetic field measurements is an inverse problem, often called "impedance tomography", "electromagnetic induction tomography", "magnetotellurics" and so on. Applications arise in many areas, for example in medicine with diagnostic imaging, in nondestructive testing, in oil recovery, in subsurface flow monitoring, in underground contaminant detection, etc. In this paper we will focus attention on imaging heterogeneous media with large variations in the magnitude of their electrical properties. This is relevant in many geophysical applications where the conductivity can vary over several orders of magnitude. For example, a dry rock matrix is insulating compared to liquid filled pores. Some pore liquids, such as hydrocarbons, are poor conductors in comparison with other pore liquids, such as brines [4, 33]. Thus, the subsurface conductivity can have very large variations, even at macroscopic length scales where some averaging is built into the model.

Mathematically, we have to consider direct and inverse problems for elliptic systems of linear partial differential equations with high contrast coefficients. Inverse problems for such partial differential equations are highly nonlinear and pose difficult analytical and computational questions. In particular, standard imaging methods that use some form of linearization about a reference medium (Born approximation) [1, 15, 21, 43] are not appropriate for imaging high contrast media. Nonlinear output least squares [47, 32] and nonlinear variational methods [37] can fail as well.

For imaging high contrast media we take a different approach. We combine asymptotic methods and recently introduced variational principles to give an accurate and efficient description of the behavior of the fields in the region of

* Work supported by AFOSR grant F49620-98-1-0211 and by NSF grant DMS-9971972

interest. We show in particular that transport properties of high contrast media can be well approximated by electrical networks. Discrete circuit approximations of continuum conductivity problems have been considered in the past [20, 18, 19], where the resistor networks are numerical discretizations of the partial differential equations. The networks considered in this study are radically different. They arise from the strong channeling of currents in materials that have large variations of electrical conductivity and/or permittivity. In this paper, we review and build upon our results in [9, 11, 10, 8] to justify rigorously network approximations of static and quasi-static electromagnetic transport in high contrast media. In the static case, we have resistor networks whereas at nonzero frequency, we have resistor-capacitor or resistor-inductor networks, depending on the properties of the high contrast media. Data available in inversion applications in high contrast media contain information mostly about the asymptotic networks. Therefore imaging high contrast media reduces mainly to imaging these networks.

We begin with the time-harmonic Maxwell's equations [31]

$$\begin{aligned} \nabla \times \mathbf{H}(\mathbf{x},\omega) &= [\sigma(\mathbf{x}) - i\omega\varepsilon(\mathbf{x})]\,\mathbf{E}(\mathbf{x},\omega), \\ \nabla \times \mathbf{E}(\mathbf{x},\omega) &= i\omega\mu(\mathbf{x})\mathbf{H}(\mathbf{x},\omega), \\ \nabla \cdot [\varepsilon(\mathbf{x})\mathbf{E}(\mathbf{x},\omega)] &= 0, \\ \nabla \cdot [\mu(\mathbf{x})\mathbf{H}(\mathbf{x},\omega)] &= 0 \ , \end{aligned} \tag{1}$$

where $\mathbf{H}$ and $\mathbf{E}$ are the complex magnetic and electric fields, $i = \sqrt{-1}$, σ is the electrical conductivity, ε is the electric permittivity, μ is the magnetic permeability and ω is the frequency. The excitation is given by some form of nonhomogeneous boundary conditions. For example, in impedance tomography the excitation consists of the current flux $\mathbf{j} = \nabla \times \mathbf{H}$ normal to the boundary. In electromagnetic induction tomography the excitation consists of magnetic dipoles at the boundary. We consider only low frequencies and distinguish three different elliptic problems to study:

1. Static ($\omega = 0$) conducting media. We study the *d.c. impedance tomography problem.*
2. Quasistatic dielectric media, where the magnetic term $i\omega\mu\mathbf{H}$ in (1) is negligible. The resulting problem has a: *complex conductivity.*
3. Quasistatic conductive media, where the displacement current $i\omega\varepsilon\mathbf{E}$ is negligible. The resulting problem is: *inductive.*

Our theory applies to a simply connected domain $\Omega \subset \mathbb{R}^2$. Extensions to three dimensions can be done in some cases (see for example [34] for a local, asymptotic analysis).

2 High Contrast D.C. Impedance Tomography

2.1 Formulation of the Problem

At zero frequency, equations (1) reduce to

$$\nabla \cdot [\sigma(\mathbf{x})\nabla\phi(\mathbf{x})] = 0 \quad \text{in } \Omega \ , \tag{2}$$

which we consider with Neumann boundary conditions

$$\sigma \frac{\partial \phi(\mathbf{x})}{\partial n} = I(\mathbf{x}) \quad \text{on } \partial\Omega, \quad \int_{\partial\Omega} I(s)ds = 0 \ , \tag{3}$$

Here, $\mathbf{E}(\mathbf{x}) = -\nabla\phi(\mathbf{x})$, n is the outward normal to the boundary $\partial\Omega$ and I is the normal current density given at the boundary. In impedance tomography $\sigma(\mathbf{x})$ is unknown and it is to be found from simultaneous measurements of currents and voltages at the boundary. Thus, for a given current excitation I we overspecify problem (2) by requiring that

$$\phi(\mathbf{x}) = \psi(\mathbf{x}) \quad \text{on } \partial\Omega \ , \tag{4}$$

where ψ is the measured voltage at the boundary. When all possible excitations and measurements at the boundary are available then we know the Neumann to Dirichlet (NtD) map which maps current I into voltages ψ at the boundary. The mathematical problem of impedance tomography is to find σ in the interior of Ω, from the NtD map. In practice, we rarely have the full NtD map available, so the imaging has to be done with partial, noisy information about it. The inverse problem can also be formulated in terms of the Dirichlet to Neumann (DtN) map which maps voltages into currents. In this case, we design our data gathering experiments so that we specify the voltage at the boundary and measure currents.

We assume that σ has high contrast, which means that the ratio of its maximum to its minimum value is large. There are many ways in which high contrast may arise in conducting media. We can have, for example, media with insulating or highly conducting inclusions in a smooth background. Since in most applications we do not have detailed information about the medium, such as the shape of inclusions, we model high contrast conductivity as a continuous function given by

$$\sigma(\mathbf{x}) = \sigma_0 e^{-S(\mathbf{x})/\epsilon} \ , \tag{5}$$

where σ_0 is constant, $S(\mathbf{x})$ is a smooth function with isolated, nondegenerate critical points (a Morse function) and ϵ is a small and positive parameter. Thus, as ϵ decreases, the contrast of σ becomes exponentially large.

The NtD and DtN maps have been studied extensively. See for example [2, 45, 29] for discussion of important questions such as injectivity, continuity of the maps and their inverse, etc. In this section, we address a new question: How do the NtD and DtN maps behave in the asymptotic limit of infinitely high contrast or, equivalently, $\epsilon \to 0$? The DtN map $\Lambda^\epsilon : \mathrm{H}^{\frac{1}{2}}(\partial\Omega) \to \mathrm{H}^{-\frac{1}{2}}(\partial\Omega)$, is defined by

$$\Lambda^\epsilon \psi = \sigma_0 e^{-S(\mathbf{x})/\epsilon} \left. \frac{\partial \phi}{\partial n} \right|_{\partial\Omega} = I(s) \ , \tag{6}$$

where $\mathbf{n}$ is the unit outer normal to $\partial\Omega$ and ϕ is the solution of (2) with Dirichlet boundary conditions (4), for a given $\psi \in \mathrm{H}^{\frac{1}{2}}(\partial\Omega)$. Λ^ϵ is selfadjoint, positive semidefinite [45] and its quadratic form has the Dirichlet variational formulation [17]

$$(\psi, \Lambda^\epsilon \psi) = \int_{\partial\Omega} I(s)\psi(s)ds = \min_{\phi|_{\partial\Omega}=\psi} \int_\Omega \sigma_0 e^{-S(\mathbf{x})/\epsilon} \ \nabla\phi(\mathbf{x}) \cdot \nabla\phi(\mathbf{x}) \, d\mathbf{x} \ . \tag{7}$$

The generalized inverse of the map Λ^ϵ, the NtD map, $(\Lambda^\epsilon)^{-1} I = \psi$, is defined on the restricted space of currents $I \in \mathrm{H}^{-\frac{1}{2}}(\partial\Omega)$ that satisfy $\int_{\partial\Omega} I(s)ds = 0$. The NtD map is selfadjoint and positive definite and its quadratic form has the Thomson variational formulation [17]

$$(I, (\Lambda^\epsilon)^{-1} I) = \int_{\partial\Omega} I(s)\psi(s)ds = \min_{\substack{\nabla\cdot\mathbf{j}=0 \\ -\mathbf{j}\cdot\mathbf{n}\,|_{\partial\Omega} = I}} \int_\Omega \frac{1}{\sigma_0} e^{S(\mathbf{x})/\epsilon}\, \mathbf{j}(\mathbf{x})\cdot\mathbf{j}(\mathbf{x})\, d\mathbf{x} \ , \tag{8}$$

where $\mathbf{j}$ is the current density. We conclude this section with the observation that at their minima, both variational principles (7) and (8) give the same result, $\int_{\partial\Omega} I(s)\psi(s)ds$, which is physically the power dissipated into heat in the conducting medium.

2.2 Asymptotic Resistor Network Approximation

In [11, 10] we carry out an asymptotic analysis of the elliptic problem (2) in a high contrast medium with conductivity (5). We show that static transport in such a high contrast continuum can be approximated by current flow through a resistor network. The network topology is uniquely defined by ridges of maximal conductivity (5), in the domain of the solution. Suppose that the high contrast conductivity (5) has the set $\mathcal{N}_I$ of N_I maxima in the interior of Ω. These are the interior nodes of the resistor network. Suppose that the ridges of maximal conductivity intersect the boundary at a set $\mathcal{N}_B$ of N_B points. These are the peripheral nodes of the network. A branch of the network connects two adjacent nodes through a saddle point, say $\mathbf{x}_S$ with resistance

$$R(\mathbf{x}_s) = \frac{1}{\sigma(\mathbf{x}_s)}\sqrt{\frac{k_1}{k_2}} \ . \tag{9}$$

To get this asymptotic resistance at the saddle we use the local Taylor series expansion of the scaled logarithm of σ

$$S(\mathbf{x}) = S(\mathbf{x}_s) + \frac{k_1}{2}y^2 - \frac{k_2}{2}x^2 + \dots \ , \tag{10}$$

where we consider a system of coordinates centered at $\mathbf{x}_s$, with axis x pointing along the ridge of maximal σ passing through $\mathbf{x}_s$. We complete the definition of the asymptotic network by defining the potential and current excitations, given an arbitrary potential $\psi(s)$ and normal current $I(s)$ measured at arclength s along the boundary $\partial\Omega$ of the high contrast continuum. Consider a peripheral node $j \in \mathcal{N}_B$ that is located at s_j on $\partial\Omega$. In [10], we show that the network potential at node j is

$$\Psi_j = \psi(s_j) \ . \tag{11}$$

To calculate the current $\mathcal{I}_j$, flowing into node j, we focus attention on the maximum of σ, say $\mathbf{x}_M$ that is adjacent to s_j. We define the basin of attraction of

$\mathbf{x}_M$ as the region in Ω that contains $\mathbf{x}_M$ and lies between $\partial\Omega$ and the nearby ridges of minimal σ. Suppose that these ridges intersect $\partial\Omega$ at points s_{j_1} and s_{j_2}. Clearly, s_j lies between s_{j_1} and s_{j_2} and, as shown in [10],

$$\mathcal{I}_j = \int_{s_{j_1}}^{s_{j_2}} I(s)ds \ . \tag{12}$$

This means that the input current at node $j \in \mathcal{N}_B$ in the asymptotic network is the net current flowing into the basin of attraction of the maximum $\mathbf{x}_M$, adjacent to peripheral node j. Results (12) and (11) are proved rigorously in [10] and they allow us to calculate all peripheral network currents $\boldsymbol{\mathcal{I}} = (\mathcal{I}_1, \mathcal{I}_2, \ldots \mathcal{I}_{N_B})^T$ and potentials $\boldsymbol{\Psi} = (\Psi_1, \Psi_2, \ldots \Psi_{N_B})^T$.

In figure 1, we show an example of how the asymptotic resistor network is constructed. We consider a continuum with a high contrast conductivity that has four maxima and six minima shown in the figure by $x_a, \ldots x_d$ and $x_{a'}, \ldots x_{f'}$, respectively. There are also five saddle points of σ denoted in the figure by $1, \ldots 5$. The current flows along paths of maximal conductivity, shown in figure 1 with a full line. Each maximum of σ has a basin of attraction delimited in Ω by the ridge of minimal conductivity passing through the neighboring saddle points (the dotted curves in figure 1). Because of the external driving, the current must flow from one maximum of σ to another with the least resistive path goes through the saddle points. When the contrast of σ is high, the current is strongly concentrated along the paths of maximal conductivity and so it flows like current in a resistor network. The branches of the network connect adjacent maxima of σ through the saddle points. Thus, in figure 1 we have five branches, each with resistance R_i, $i = 1, \ldots 5$. We also have four peripheral nodes a, b, c and d, where $\partial\Omega$ intersects ridges of maximal σ. The asymptotic resistor network is shown in figure 1. The network excitation at the peripheral node a is defined as in (11) and (12): $\Psi_a = \psi(s_a)$ and $\mathcal{I}_a = \int_{s_{a'}}^{s_{b'}} I(s)ds$, respectively.

The discrete DtN map $\Lambda^{D,\epsilon}$ is a symmetric $N_B \times N_B$ positive semidefinite matrix with a null space spanned by the vector $(1, 1, \ldots 1)^T \in \mathbb{R}^{N_B \times 1}$. This matrix gives the input/output current in terms of the boundary potential,

$$\mathcal{I}_j = \sum_{k \in \mathcal{N}_B} \Lambda^{D,\epsilon}_{jk} \Psi_k, \qquad \text{for all } j \in \mathcal{N}_B \ . \tag{13}$$

Its quadratic form has the variational formulation

$$< \boldsymbol{\Psi}, \Lambda^{D,\epsilon} \boldsymbol{\Psi} > = \sum_{j \in \mathcal{N}_B} \mathcal{I}_j \Psi_j = \min_{\Phi_k = \Psi_k \text{ if } k \in \mathcal{N}_B} \frac{1}{2} \sum_{j \in \mathcal{N}} \sum_{k \in \mathcal{V}_j} \frac{1}{R^\epsilon_{jk}} (\Phi_j - \Phi_k)^2 \ . \tag{14}$$

Here, $\mathcal{V}_j$ is the set of neighbors of node j in the set $\mathcal{N} = \mathcal{N}_I \bigcup \mathcal{N}_B$. The resistance R^ϵ_{jk} is given by (9), where $\mathbf{x}_s$ is the saddle point that connects the maxima $\mathbf{x}_j$ and $\mathbf{x}_k$ of σ or, equivalently, the nodes j and k in the network. The superscript ϵ reminds us that the resistance depends on the small parameter ϵ because of

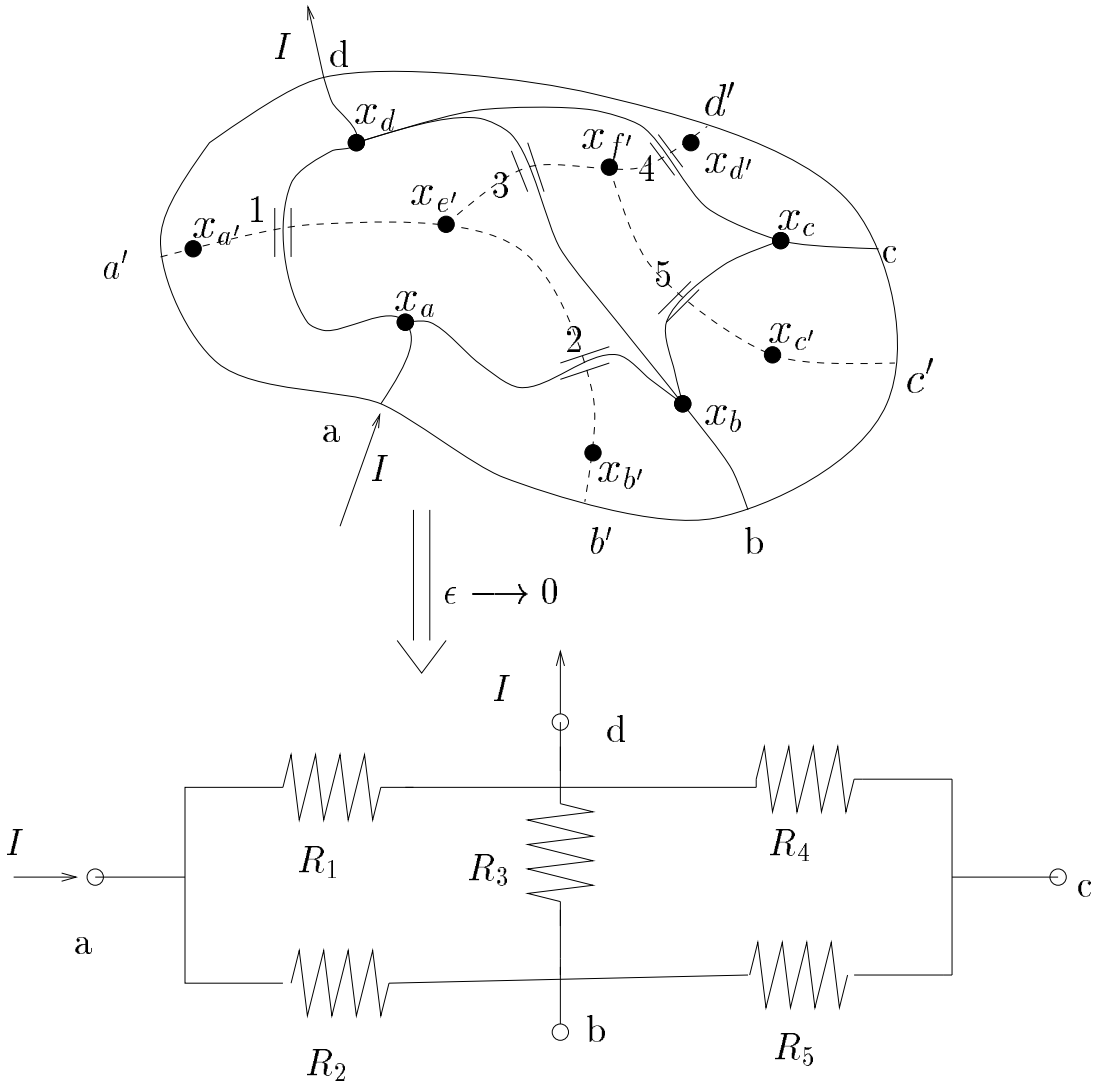

Fig. 1. Example of an asymptotically equivalent resistor network

the factor $\sigma(\mathbf{x}_s) = \sigma_0 e^{-\frac{S(\mathbf{x}_s)}{\epsilon}}$. The pseudoinverse of $\Lambda^{D,\epsilon}$ is the NtD map that gives the boundary potentials in terms of the currents,

$$\Psi_j = \sum_{k \in \mathcal{N}_B} (\Lambda^{D,\epsilon})^{-1}_{jk} \mathcal{I}_k, \quad \text{for all } j \in \mathcal{N}_B \ . \tag{15}$$

The domain of the map $(\Lambda^{D,\epsilon})^{-1}$ is the $N_B - 1$ dimensional space spanned by current vectors $\boldsymbol{\mathcal{I}} = (\mathcal{I}_1, \mathcal{I}_2, \ldots \mathcal{I}_{N_B})^T \in R^{N_B \times 1}$ that satisfy the constraint (13). $(\Lambda^{D,\epsilon})^{-1}$ is symmetric, positive definite and its quadratic form has the following variational formulation

$$< \boldsymbol{\mathcal{I}}, (\Lambda^{D,\epsilon})^{-1} \boldsymbol{\mathcal{I}} >= \sum_{j \in \mathcal{N}_B} \mathcal{I}_j \Psi_j = \min_{J_{jk}} \frac{1}{2} \sum_{j \in \mathcal{N}} \sum_{k \in \mathcal{V}_j} R^{\epsilon}_{jk} J^2_{jk} \ . \tag{16}$$

Here the currents J_{jk} satisfy Kirchhoff's nodal law

$$\sum_{k \in \mathcal{V}_j} J_{jk} = \begin{cases} 0 & \text{if } j \in \mathcal{N}_I, \\ \mathcal{I}_j & \text{if } j \in \mathcal{N}_B \ . \end{cases} \tag{17}$$

2.3 Asymptotics and the Variational Principles

We will analyze briefly the quadratic forms $(\psi, \Lambda^{\epsilon}\psi)$ and $(I, (\Lambda^{\epsilon})^{-1} I)$ of the DtN and NtD maps in media with conductivity (5), in the asymptotic limit $\epsilon \to 0$. We show that, as $\epsilon \to 0$, we have

$$\begin{aligned} (\psi, \Lambda^{\epsilon}\psi) &= < \boldsymbol{\Psi}, \Lambda^{D,\epsilon} \boldsymbol{\Psi} > [1 + o(1)] \, , \\ (I, (\Lambda^{\epsilon})^{-1} I) &= < \boldsymbol{\mathcal{I}}, (\Lambda^{D,\epsilon})^{-1} \boldsymbol{\mathcal{I}} > [1 + o(1)] \ . \end{aligned} \tag{18}$$

The proof of (18) relies on the variational principles (7) and (8). We obtain upper and lower bounds on the quadratic forms $(\psi, \Lambda^{\epsilon}\psi)$ and $(I, (\Lambda^{\epsilon})^{-1} I)$ and show that these bounds match asymptotically and are equal to the right hand sides in (18). To simplify the exposition here, let us assume that we have a boundary current I that is concentrated precisely at the peripheral nodes of the asymptotic network. Of course, in a real experiment the current excitation is unlikely to satisfy this assumption. In [10], we show how to handle the case of arbitrary $I \in \mathrm{H}^{-\frac{1}{2}}(\partial\Omega)$. We introduce a thin layer near the boundary, where the current adjusts from the given I along $\partial\Omega$ to the current concentrated along ridges of maximal σ in the interior of Ω. We show that the contribution of this layer to $(I, (\Lambda^{\epsilon})^{-1} I)$ is negligible as $\epsilon \to 0$. The analysis is done in [10] and shall not be repeated here.

To get an upper bound on $(I, (\Lambda^{\epsilon})^{-1} I)$ we take in (8) a trial field

$$\mathbf{j}(x) = \left(-\frac{\partial}{\partial y}, \frac{\partial}{\partial x} \right) H(x, y) \ , \tag{19}$$

such that, at the boundary, $-\mathbf{j}(s) \cdot \mathbf{n}(s) = I(s) = \frac{\partial H}{\partial s}$, where we assume that I is concentrated at $s_j \in \partial\Omega$, for $j \in \mathcal{N}_B$. Thus, we have the Dirichlet boundary condition

$$H(s) = \int^s I(t) dt, \quad \text{on } \partial\Omega \ , \tag{20}$$

where H is constant along pieces of $\partial\Omega$ that lie between two adjacent peripheral nodes of the network. In the interior of Ω, away from the ridges of maximal conductivity, we take H to be a constant.

Along the ridges of maximal σ we expect strong, concentrated currents. Consider such a ridge of maximal conductivity and introduce curvilinear coordinates (ξ,η), with ξ arclength along the ridge. For $\mid \eta \mid \leq \delta \ll 1$, such that $\frac{\delta^2}{\epsilon} \to \infty$ as $\epsilon \to 0$, we have $\sigma(\xi,\eta) = \sigma_0 e^{-S(\xi,\eta)/\epsilon}$, where

$$S(\xi,\eta) = S(\xi,0) + \frac{k(\xi)}{2}\eta^2 + \frac{1}{6}\frac{\partial^3 S}{\partial\eta^3}(\xi,0)\eta^3 + \frac{1}{24}\frac{\partial^4 S}{\partial\eta^4}(\xi,0)\eta^4 + \dots \ . \tag{21}$$

Here $k(\xi)$ is the curvature in the direction η and, by our assumption of a conductivity function with non degenerate critical points, $k(\xi) > 0$. We take

$$H(\xi,\eta) = -\frac{f}{2}\ \mathrm{erf}\ \left(\frac{\eta}{\sqrt{\frac{2\epsilon}{k(\xi)}}}\right) + \text{ constant } , \tag{22}$$

where, f is the net current flowing along the ridge. Then, as shown in [10],

$$\begin{aligned}\mathbf{j}(\xi,\eta) &= \frac{f}{\sqrt{2\pi\epsilon}} e^{-\frac{k(\xi)\eta^2}{2\epsilon}} \left[\sqrt{k(\xi)}\hat{\xi} - \frac{\eta}{2\sqrt{k(\xi)}}\frac{dk(\xi)}{d\xi}\left(1+O(\delta)\right)\hat{\eta}\right] \\ &\approx \frac{f\sqrt{k(\xi)}}{\sqrt{2\pi\epsilon}} e^{-\frac{k(\xi)\eta^2}{2\epsilon}}\hat{\xi} \ ,\end{aligned} \tag{23}$$

where $\hat{\xi}$ and $\hat{\eta}$ are the unit tangential and normal vectors along the ridge, respectively. We have

$$\int_\Omega \frac{1}{\sigma(\mathbf{x})}|\mathbf{j}(\mathbf{x})|^2 d\mathbf{x} = \sum_{\text{ridges in } \Omega} \int_{\text{ridge}} \frac{1}{\sigma_0} e^{S(\xi,\eta)/\epsilon} \mid \mathbf{j}(\xi,\eta) \mid^2 d\xi d\eta \ , \tag{24}$$

where we sum over all ridges of maximal conductivity in Ω. The technical details of the calculation of the integrals in (24) are given in [10]. After integration in η, we have

$$\int_{\text{ridge}} \frac{1}{\sigma_0} e^{S(\xi,\eta)/\epsilon} \mid \mathbf{j}(\xi,\eta) \mid^2 d\xi d\eta = \frac{1+O(\delta)}{\sigma_0}\int_{\xi_{in}}^{\xi_{out}} \sqrt{\frac{k(\xi)}{2\pi\epsilon}}[f(\xi)]^2 e^{\frac{S(\xi,0)}{\epsilon}} d\xi \ . \tag{25}$$

The integral (25) is of Laplace type [5] and the main contribution comes from the maxima of $S(\xi,0)$ or, equivalently, the saddle points of σ. Consider a saddle point $\mathbf{x}_S = (\xi_S, 0)$ along the ridge. In the vicinity of $\mathbf{x}_S$, $S(\xi,0)$ is given by

$$S(\xi,0) = S(\mathbf{x}_S) - \frac{p(\mathbf{x}_S)(\xi-\xi_S)^2}{2} + \frac{(\xi-\xi_S)^3}{6}\frac{\partial^3 S}{\partial\xi^3}(\xi_S,0) + \dots \ , \tag{26}$$

where $p(\mathbf{x}_S) > 0$ is the curvature of the function S at the saddle point in the direction $\hat{\xi}$. The contribution of this saddle point to the integral in (25) is

$$\frac{(1+O(\delta))}{\sigma_0}\int_{\xi-\xi_S}^{\xi+\xi_S} e^{\frac{S(\mathbf{x}_S)}{\epsilon}-\frac{p(\mathbf{x}_S)(\xi-\xi_S)^2}{2\epsilon}+\frac{(\xi-\xi_S)^3}{6\epsilon}\frac{\partial^3 g}{\partial\xi^3}(\xi_S)+\cdots}\sqrt{\frac{k(\xi)}{2\pi\epsilon}}[f(\xi)]^2 d\xi$$
$$= \frac{[f(\mathbf{x}_S)]^2}{\sigma(\mathbf{x}_S)}\sqrt{\frac{k(\mathbf{x}_S)}{p(\mathbf{x}_S)}}(1+O(\delta)) \quad ,$$

where $f(\mathbf{x}_S)$ is the net current through the saddle. We now add the contribution of all saddle points along the ridge and, since $\delta \ll 1$, we obtain

$$\int_{\text{ridge}} \frac{1}{\sigma_0} e^{S(\xi,\eta)/\epsilon} \mid \mathbf{j}(\xi,\eta) \mid^2 d\xi d\eta = \sum_{\mathbf{x}_S \in \text{ ridge}} [f(\mathbf{x}_S)]^2 R(\mathbf{x}_S)(1+o(1)) \quad , \tag{27}$$

where $R(\mathbf{x}_S) = \frac{1}{\sigma(\mathbf{x}_S)}\sqrt{\frac{k(\mathbf{x}_S)}{p(\mathbf{x}_S)}}$ is the effective resistance of saddle $\mathbf{x}_S$.

The upper bound is thus

$$(I,(\Lambda^\epsilon)^{-1}I) \leq \min_f \sum_{\mathbf{x}_S} [f(\mathbf{x}_S)]^2 R(\mathbf{x}_S)(1+o(1)) =< \boldsymbol{\mathcal{I}}, (\Lambda^{D,\epsilon})^{-1}\boldsymbol{\mathcal{I}} > [1+o(1)] \quad . \tag{28}$$

Note that because of conservation of currents in Ω the minimization in (28) is done over all fluxes f that satisfy Kirchhoff's nodal law for currents. A similar calculation leads to the upper bound

$$(\psi, \Lambda^\epsilon \psi) \leq < \boldsymbol{\Psi}, \Lambda^{D,\epsilon}\boldsymbol{\Psi} > [1+o(1)] \quad , \tag{29}$$

where we use variational principle (7). Using the convex duality relation

$$(\psi, \Lambda^\epsilon \psi) = \sup_{I \in \mathrm{H}^{-\frac{1}{2}}(\partial\Omega)} \left[2(I,\psi) - (I,(\Lambda^\epsilon)^{-1}I)\right] \quad , \tag{30}$$

we obtain lower bounds on $(\psi, \Lambda^\epsilon\psi)$ and $(I,(\Lambda^\epsilon)^{-1}I)$. These lower bounds match asymptotically the upper bounds (28) and (29), respectively and the proof is complete. The details are given in [10].

2.4 How to Chose the Test Functions

The results presented in section 2.3 show that static conductive transport in high contrast media is asymptotically equivalent to current flow in a resistor network, uniquely determined by the conductivity (5). This asymptotic network approximation comes from the strong channeling of currents along ridges of maximal σ, given by (5). The proof of the asymptotic resistor network approximation, given in [10] and in section 2.3, relies entirely on the variational principles (7) and (8) and a careful choice of trial fields. We now give a brief explanation of how we found these trial fields by looking directly at the governing equations in Ω.

The current density

$$\mathbf{j}(\mathbf{x}) = -\sigma(\mathbf{x})\nabla\phi(\mathbf{x}) = \nabla^\perp H(x,y) \ , \tag{31}$$

where $\nabla^\perp = \left(-\frac{\partial}{\partial y}, \frac{\partial}{\partial x}\right)$, is the minimizer of (8) if

$$\nabla^\perp \cdot \left[\frac{1}{\sigma_0} e^{S(\mathbf{x})/\epsilon} \nabla^\perp H(\mathbf{x})\right] = 0 \quad \text{in } \Omega,$$
$$H(s) = \int^s I(s)ds, \qquad \text{on } \partial\Omega \ . \tag{32}$$

Thus, we have the singularly perturbed problem [36]

$$\Delta H(\mathbf{x}) + \frac{1}{\epsilon}\nabla S(\mathbf{x}) \cdot \nabla H(\mathbf{x}) = 0 \quad \text{in } \Omega \ . \tag{33}$$

Consider $\mathbf{x} \in \Omega$ that is neither a minimum nor a maximum or a saddle point of σ that is, $\nabla S(\mathbf{x}) \neq \mathbf{0}$. Then, $H(\mathbf{x})$ satisfies approximately,

$$\nabla S(\mathbf{x}) \cdot \nabla H(\mathbf{x}) = 0 \ , \tag{34}$$

or, equivalently, H varies in directions orthogonal to $\nabla S(\mathbf{x})$. The current $\mathbf{j}(\mathbf{x}) = \nabla^\perp H(\mathbf{x})$ is orthogonal to $\nabla H(\mathbf{x})$ so, it is parallel to $\nabla S(\mathbf{x})$. In fact, $\mathbf{j}(\mathbf{x})$ points in direction $-\nabla S(\mathbf{x})$, towards higher conductivity, in order to achieve the minimum in (8).

Let us begin with points near the boundary and justify the result (12). To fix ideas we take the situation of figure 1 and focus attention on the basin of attraction of x_a, a maximum of σ. From (34) the current density $\nabla^\perp H$ flows from the boundary downhill towards x_a, the closest point of minimum resistance $\rho(\mathbf{x}) = \frac{1}{\sigma_0} e^{S(\mathbf{x})/\epsilon}$ (see figure 2). The net current flowing into x_a is $\mathcal{I}_a = \int_{s_{a'}}^{s_{b'}} I(s)ds$, as given by formula (12). At x_a, $\nabla S = 0$ and equation (34) is not valid. Here, we have an inner layer [36] of width $\delta \gg \sqrt{\epsilon}$, where H changes rapidly, as shown in [11]. Because of the external driving we have current flow from one point of minimal resistance to another. To achieve the minimum in (8) the flow goes along the least resistive paths in Ω. These paths are precisely the ridges of maximal σ that define the topology of the asymptotic network. Take for example the ridge in (21). Here,

$$\nabla S(\xi,\eta) = \left[\frac{\partial S}{\partial \xi}(\xi,0) + \frac{k'(\xi)\eta^2}{2} + \ldots\right]\hat{\xi} + k(\xi)\eta\hat{\eta} \approx \frac{\partial S}{\partial \xi}(\xi,0)\hat{\xi}$$

and, by (34), $\nabla^\perp H$ is in direction $\hat{\xi}$ tangent to the ridge. Clearly, as seen from (25), most power is dissipated as current passes through the points of highest resistance along ridges of maximal conductivity, the saddle points of σ.

In the asymptotic limit $\epsilon \to 0$ the solution of (32) is now as follows: In Ω, H changes rapidly, on a length scale of order $\sqrt{\epsilon}$, across ridges of maximal

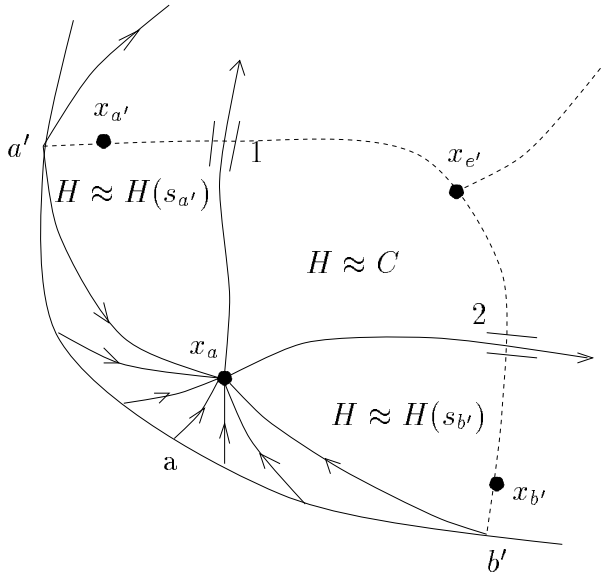

Fig. 2. Current flows from the boundary into the maximum x_a of σ, along paths of steepest descent. In the interior of Ω, current concentrates along paths of maximal conductivity

conductivity. Note that in [11] we do the local asymptotic analysis of (32) near saddle points of σ and find that H is of the form (22). In the rest of Ω, except possibly for thin boundary layers, H is approximately a constant, as shown in figure 2. Here, to the left of the network branch that passes through saddle point 1 we have $H \approx H(s_{a'})$, where $s_{a'}$ is arclength along $\partial\Omega$ at a', the intersection of the boundary with the ridge of minimal conductivity through $x_{a'}$. Similarly, below the branch through the saddle point 2 we have $H \approx H(s_{b'})$. In the interior of Ω between the two branches of figure 2 $H \approx C$, a constant, and so on. The actual constant values of H in the interior of Ω cannot be calculated from a local asymptotic analysis. For this, we need to study the global problem and the tools for that are variational principles (7) and (8).

Singular perturbation methods [36] applied to (32) give us a physically clear picture of static transport in high contrast media. Our proof in section 2.3 relies entirely on the variational principles (7) and (8) and it needs no further justification. However, the key to the successful use of the variational principles is, of course, having good trial fields. The local asymptotic analysis presented here is precisely the guide to finding these trial fields.

2.5 Imaging High Contrast Media

The results summarized in section 2.2 show that imaging high contrast σ of the form (5) is asymptotically equivalent to the identification of a resistor network

from measurements of currents and voltages at the peripheral nodes. Therefore, in high contrast inversion the most important features of the conductivity are near the saddle points. Each saddle point of σ corresponds to a resistor in the asymptotic network and makes a significant contribution to the quadratic forms $(\psi, \Lambda^\epsilon \psi)$ and $(I, (\Lambda^\epsilon)^{-1} I)$ or, equivalently, to the eigenvalues of the DtN and NtD maps. The location of maxima and minima of σ in Ω determine the current flow topology and so they influence the spectra of the DtN and NtD maps. The actual value of σ at the maxima and minima is not so important in the asymptotic limit. Therefore, when imaging a high contrast conductivity (5) we cannot expect a good estimate of the value of σ at the minima or maxima. We should get, however, a good image at the saddle points as well as a fair estimate of the location of all critical points. The question of the unique recovery of resistor networks from the discrete DtN or NtD maps has been considered in [18, 24, 19]. It is shown there that, in general, rectangular resistor networks can be uniquely recovered. Even more general resistor networks can be uniquely recovered up to $Y - \Delta$ transformations (see [19] for details). However, the question of how to image these networks in practice does not have a satisfactory answer so far, especially when the network topology is not known apriori. In [9, 10], we propose imaging asymptotic resistor networks with the method of matching pursuit [41]. We show with extensive numerical computations that matching pursuit is effective in imaging high contrast conductive media if the library of functions is carefully constructed to capture the features of σ that come from the asymptotic theory.

3 Quasi-Static Approximation: Complex Conductivity

In dielectric media at low frequency the magnetic term $i\omega\mu\mathbf{H}$ in (2) can be neglected [11]. In two dimensions, the magnetic field $\mathbf{H}(\mathbf{x}) = H(\mathbf{x})\mathbf{e}_3$, $H = H_R + i\, H_I$, satisfies

$$\begin{aligned} \nabla^\perp \cdot \left\{ [\rho(\mathbf{x}) + i\, \mathcal{C}(\mathbf{x})]\, \nabla^\perp H(\mathbf{x}) \right\} = 0, \quad \mathbf{x} \in \Omega \subset \mathbb{R}^2, \\ -\nabla^\perp H(\mathbf{x}) \cdot \mathbf{n}(\mathbf{x}) = I(\mathbf{x}) = I_R(\mathbf{x}) + i\, I_I(\mathbf{x}) \quad \text{on } \partial\Omega, \\ \int_{\partial\Omega} I(s) ds = 0 \ , \end{aligned} \tag{35}$$

where $\rho + i\, \mathcal{C}$ is the complex impedance consisting of the resistance(real part) $\rho = \frac{\sigma}{\sigma^2 + \omega^2 \varepsilon^2}$ and the capacitive reactance (imaginary part) $\mathcal{C} = \frac{\omega\varepsilon}{\sigma^2 + \omega^2 \varepsilon^2}$. We define the current density

$$\mathbf{j}(\mathbf{x}) = \mathbf{j}_R(\mathbf{x}) + i\, \mathbf{j}_I(\mathbf{x}) = \nabla^\perp H(\mathbf{x}) \ , \tag{36}$$

such that $\nabla \cdot \mathbf{j}(\mathbf{x}) = 0$ for all $\mathbf{x} \in \Omega$ and, at the boundary, $-\mathbf{j}(\mathbf{x}) \cdot \mathbf{n}(\mathbf{x}) = I(\mathbf{x})$. Equation (35) implies that

$$\nabla \phi(\mathbf{x}) = -\left[\rho(\mathbf{x}) + i\, \mathcal{C}(\mathbf{x})\right] \mathbf{j}(\mathbf{x}), \quad \mathbf{x} \in \Omega \ , \tag{37}$$

where ϕ is the complex electric potential. In the inverse problem of complex conductivity, $\rho(\mathbf{x})$ and $\mathcal{C}(\mathbf{x})$ are unknown and are to be found from simultaneous measurements of currents and potentials at the boundary. Thus, for a given current excitation I we overspecify problem (35) by asking that

$$\phi(\mathbf{x}) = \psi(\mathbf{x}) \quad \text{on } \partial\Omega \quad , \tag{38}$$

where ψ is the complex potential measured at the boundary. When all possible excitations and measurements at the boundary are available, then we know the complex Neumann to Dirichlet (NtD) map which takes I and maps it into ψ. In most applications we do not have full knowledge of the NtD map and the inversion must be done with partial, noisy information about it.

We are interested in dielectric media with high contrast and we model the complex impedance by

$$\rho(\mathbf{x}) = \rho_0 e^{-S(\mathbf{x})/\epsilon}, \quad \mathcal{C}(\mathbf{x}) = \mathcal{C}_0 e^{-P(\mathbf{x})/\epsilon} \quad , \tag{39}$$

where ρ_0 and $\mathcal{C}_0$ are constants, $S(\mathbf{x})$ and $P(\mathbf{x})$ are smooth functions with isolated, nondegenerate critical points and ϵ is a positive, small parameter. The complex NtD map $\Gamma^\epsilon = \Gamma^\epsilon_R + i\Gamma^\epsilon_I$ is defined by

$$\Gamma^\epsilon I(\mathbf{x}) = \psi(\mathbf{x}), \quad \mathbf{x} \in \partial\Omega \quad . \tag{40}$$

The domain of the NtD map is the restricted space of currents $I = I_R + iI_I$ that satisfy $I_R,\ I_I \in \mathrm{H}^{-\frac{1}{2}}(\partial\Omega)$ and $\int_{\partial\Omega} I(\mathbf{s})ds = 0$. From Green's theorem, we have

$$(I^\star, \Gamma^\epsilon I) = \int_{\partial\Omega} \psi(s) I^\star(s) ds = \int_\Omega \left[\rho_0 e^{-S(\mathbf{x})/\epsilon} + i\ \mathcal{C}_0 e^{-P(\mathbf{x})/\epsilon}\right] \mid \mathbf{j}(\mathbf{x}) \mid^2 d\mathbf{x} \quad , \tag{41}$$

where $I^\star$ is the complex conjugate of I. Thus, the eigenvalues $\lambda^\epsilon = \lambda^\epsilon_R + i\lambda^\epsilon_I$ of Γ^ϵ have strictly positive real and imaginary parts.

In order to study the NtD map in the asymptotic limit $\epsilon \to 0$, it is important to have variational formulations for quadratic forms of Γ^ϵ. For this purpose we rewrite (35) as an elliptic system of equations

$$\begin{aligned}
\nabla^\perp \cdot \left[\rho_0 e^{-S(\mathbf{x})/\epsilon} \mathbf{j}_R(\mathbf{x}) - \mathcal{C}_0 e^{-P(\mathbf{x})/\epsilon} \mathbf{j}_I(\mathbf{x})\right] &= 0, \\
\nabla^\perp \cdot \left[\rho_0 e^{-S(\mathbf{x})/\epsilon} \mathbf{j}_I(\mathbf{x}) + \mathcal{C}_0 e^{-P(\mathbf{x})/\epsilon} \mathbf{j}_R(\mathbf{x})\right] &= 0, \\
\mathbf{j}_R(\mathbf{x}) = \nabla^\perp H_R(\mathbf{x}),\ \mathbf{j}_I(\mathbf{x}) = \nabla^\perp H_I(\mathbf{x}), &\quad \text{for } \mathbf{x} \in \Omega \quad .
\end{aligned} \tag{42}$$

At the boundary, we give the normal current $-[\mathbf{j}_R(s) + i\mathbf{j}_I(s)] \cdot \mathbf{n}(s) = I(s) + i\ I_I(s)$ or, equivalently, the Dirichlet conditions

$$\begin{aligned}
H_R(s) &= \int^s I_R(s) ds, \\
H_I(s) &= \int^s I_I(s) ds \quad ,
\end{aligned} \tag{43}$$

where s is arclength along $\partial\Omega$. Equations (42) with boundary conditions (43) have a unique (at least weak) solution H_R and $H_I \in \mathrm{H}^1(\Omega)$, provided that $\rho(\mathbf{x}) > 0$ and $\rho(\mathbf{x})$ and $\mathcal{C}(\mathbf{x})$ are uniformly bounded in Ω. Equations (42) are also the Euler equations for the following saddle point variational principles [16, 22, 11]

$$\begin{aligned}
&\mathrm{real}(I, \Gamma^\epsilon I) \\
&= \min_{\substack{\nabla\cdot\mathbf{j}_R = 0 \\ -\mathbf{j}_R\cdot\mathbf{n}\,|_{\partial\Omega} = I_R}} \max_{\substack{\nabla\cdot\mathbf{j}_I = 0 \\ -\mathbf{j}_I\cdot\mathbf{n}\,|_{\partial\Omega} = I_I}} \int_\Omega \Big\{ \rho_0 e^{-S(\mathbf{x})/\epsilon} \left[|\,\mathbf{j}_R(\mathbf{x})\,|^2 - |\,\mathbf{j}_I(\mathbf{x})\,|^2 \right] - \\
&\qquad\qquad 2\mathcal{C}_0 e^{-P(\mathbf{x})/\epsilon} \mathbf{j}_R(\mathbf{x})\cdot\mathbf{j}_I(\mathbf{x}) \Big\}\, d\mathbf{x}\ , \qquad (44)
\end{aligned}$$

$$\begin{aligned}
&\mathrm{imag}(I, \Gamma^\epsilon I) \\
&= \min_{\substack{\nabla\cdot\mathbf{j}_R = 0 \\ -\mathbf{j}_R\cdot\mathbf{n}\,|_{\partial\Omega} = I_R}} \max_{\substack{\nabla\cdot\mathbf{j}_I = 0 \\ -\mathbf{j}_I\cdot\mathbf{n}\,|_{\partial\Omega} = I_I}} \int_\Omega \Big\{ \mathcal{C}_0 e^{-P(\mathbf{x})/\epsilon} \left[|\,\mathbf{j}_R(\mathbf{x})\,|^2 - |\,\mathbf{j}_I(\mathbf{x})\,|^2 \right] + \\
&\qquad\qquad 2\rho_0 e^{-S(\mathbf{x})/\epsilon} \mathbf{j}_R(\mathbf{x})\cdot\mathbf{j}_I(\mathbf{x}) \Big\}\, d\mathbf{x}\ . \qquad (45)
\end{aligned}$$

3.1 Asymptotic Resistor-Capacitor Network Approximation

In [11], we carry out an asymptotic analysis of (35) for periodic dielectric media. In this section we review the results of [11] and we extend the asymptotic analysis to more general high contrast dielectrics, not just periodic ones. We show that in the asymptotic limit $\epsilon \to 0$ the solution $\mathbf{j} = \mathbf{j}_R + i\mathbf{j}_I$ of (42) and (43) can be approximated by current flow through a resistor-capacitor network. We show further that the NtD map Γ^ϵ is asymptotically equivalent to the discrete NtD map of the resistor-capacitor network.

Let us begin with the observation that since $\epsilon \ll 1$ the resistance $\rho(\mathbf{x})$ dominates $\mathcal{C}(\mathbf{x})$ when its scaled logarithm $S(\mathbf{x})$ is less than $P(\mathbf{x})$. In fact, $\rho(\mathbf{x})$ and $\mathcal{C}(\mathbf{x})$ are comparable in magnitude only when $S(\mathbf{x}) = P(\mathbf{x}) + O(\epsilon)$. In general, one does not expect S and P to be equal over large regions of the domain and we model the medium by alternating regions of dominant resistance and capacitance. Both ρ and $\mathcal{C}$ are smooth functions so these regions are separated by interfaces along which ρ is equal to $\mathcal{C}$. In regions of dominant ρ or $\mathcal{C}$, (42) is similar to the static problem (2). Thus, transport in these regions behaves like current flow in purely resistive or capacitive networks, respectively. The main question is how to connect these networks in order to get the global resistor-capacitor network that approximates the transport properties of the high contrast medium.

Suppose, for example, that the high contrast function $\rho(\mathbf{x})$ has the six minima denoted by $\circ$ in figure 3. Its maxima are denoted by $\bullet$ and the saddle points are numbered from 1 to 7. If we consider the static problem in a medium with resistance $\rho(\mathbf{x})$ the results of section 2.2 apply and the current flows along the ridges of minimal resistance, shown with a full line in figure 3. Similarly, in

figure 4, we show an example of a high contrast function $\mathcal{C}(\mathbf{x})$ and its associated assymptotic network.

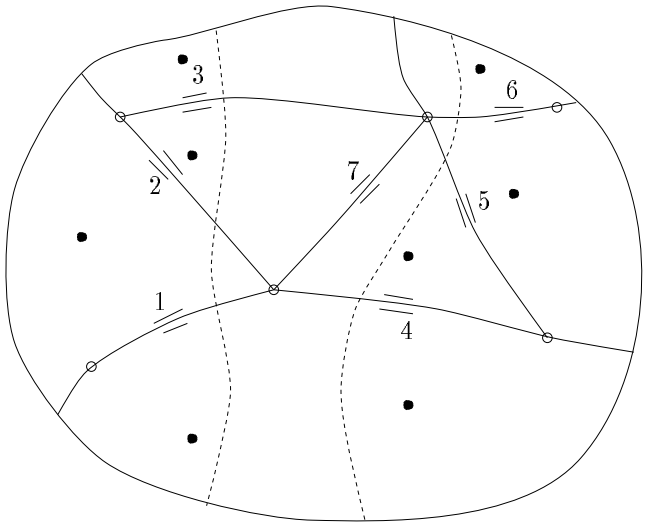

Fig. 3. The static network for an example of $\rho(\mathbf{x}) = \rho_0 e^{-S(\mathbf{x})/\epsilon}$

Consider now the complex impedance $\rho + i\mathcal{C}$. As explained above, let us suppose that $\mathcal{C}(\mathbf{x}) \gg \rho(\mathbf{x})$ for points between the dotted lines in figures 3 and 4. Along these lines (interfaces) ρ is equal to $\mathcal{C}$ and elsewhere in Ω, $\rho \gg \mathcal{C}$. Away from the interfaces we already established that (42) is similar to the static problem of section 2.1, where σ in (2) is replaced by $\frac{1}{\rho}$ if $\rho \gg \mathcal{C}$ and $\frac{1}{C}$ if $\rho \ll \mathcal{C}$, respectively. Thus, in these regions, currents flow along ridges of minimal resistance and capacitive reactance, respectively. The ridges of minimal ρ and $\mathcal{C}$ cut the interfaces, as shown in figures 3 and 4, respectively. Along the interfaces, $\rho = \mathcal{C}$ so ridges of minimal ρ and $\mathcal{C}$ must intersect the dotted lines at the same points. The network connection is now straightforward and the global network is shown in figure 5, where R_i and C_i correspond to the resistive/capacitive saddle points and they are given by formulas similar to (9). The construction illustrated in this example is general and it allows us to define the topology of the $R-C$ asymptotic network for any medium with impedance (39).

we now consider the quadratic forms $(I, \Gamma^\epsilon I)$ of the NtD map, for a high contrast impedance $\rho_0 e^{-S(\mathbf{x})/\epsilon} + i\ \mathcal{C}_0 e^{-P(\mathbf{x})/\epsilon}$, in the asymptotic limit $\epsilon \to 0$. We show that Γ^ϵ is asymptotically equivalent to $\Gamma^{D,\epsilon}$, the NtD map of the asymptotic resistor-capacitor network. First we identify the topology of the network as explained in the example of figure 5. We divide Ω into resistive regions Ω_{ρ_j}, $j = 1, \ldots N_\rho$, where $\rho \gg \mathcal{C}$ and capacitive regions Ω_{C_j}, $j = 1, \ldots N_C$, where $\mathcal{C} \gg \rho$, respectively. These regions are separated by interfaces $\mathcal{L}_j$, $j = 1, \ldots N_\mathcal{L}$,

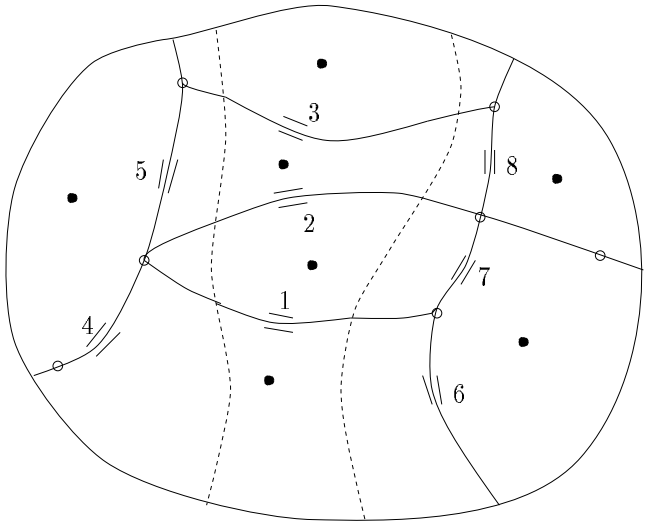

Fig. 4. The static network for an example of $\mathcal{C}(\mathbf{x}) = \mathcal{C}_0 e^{-P(\mathbf{x})/\epsilon}$

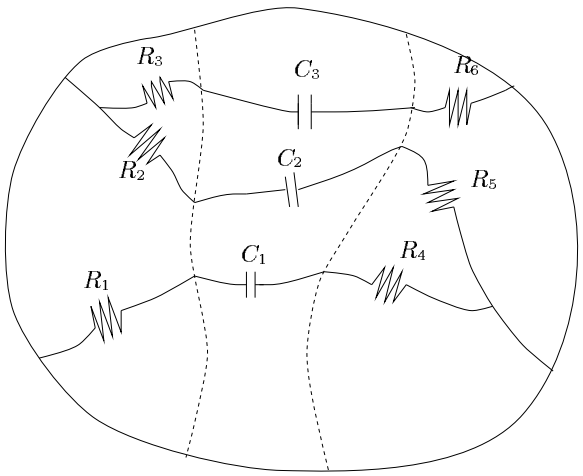

Fig. 5. The global R-C network

where $\rho = \mathcal{C}$. Suppose that the global $R-C$ network has N_B peripheral nodes, where each node corresponds to a point of intersection of $\partial\Omega$ with a ridge of minimal ρ or $\mathcal{C}$. The complex currents at the peripheral nodes are $\boldsymbol{\mathcal{I}} = (\mathcal{I}_1, \mathcal{I}_2, \ldots \mathcal{I}_{N_B})^T$. The complex electric potentials at the peripheral nodes are $\boldsymbol{\Psi} = (\Psi_1, \Psi_2, \ldots \Psi_{N_B})^T$. Take for example the point s_j of intersection of a ridge of minimal ρ with the boundary. The current flowing into this node is given by

$$\mathcal{I}_j = \int_{\partial\Omega \bigcap \overline{B}(\mathbf{x}_j)} I(s)ds \quad , \tag{46}$$

where $\overline{B}(\mathbf{x}_j)$ stands for the closure of the basin of attraction of minimum $\mathbf{x}_j$ that is adjacent to s_j. The electric potential is

$$\Psi_j = \psi(s_j) \quad . \tag{47}$$

The discrete NtD map, $\Gamma^{D,\epsilon} = \Gamma_R^{D,\epsilon} + i\ \Gamma_I^{D,\epsilon}$, is a complex $N_B \times N_B$ matrix that takes boundary currents and maps them into boundary potentials

$$\Psi_j = \sum_{k \in \mathcal{N}_B} \Gamma_{jk}^{D,\epsilon} \mathcal{I}_k, \quad \text{for all } j \in \mathcal{N}_B \quad . \tag{48}$$

We show that, given any boundary current $I = I_R + iI_I$ such that $I_R,\ I_I \in \mathrm{H}^{-\frac{1}{2}}(\partial\Omega)$ and $\int_{\partial\Omega} I(\mathbf{s})ds = 0$,

$$(I, \Gamma^\epsilon I) = < \boldsymbol{\mathcal{I}}, \Gamma^{D,\epsilon} \boldsymbol{\mathcal{I}} > [1 + o(1)] \quad , \tag{49}$$

where

$$< \boldsymbol{\mathcal{I}}, \Gamma^{D,\epsilon} \boldsymbol{\mathcal{I}} > = \sum_{j=1}^{N_B} \mathcal{I}_j \Psi_j \quad . \tag{50}$$

3.2 Asymptotics Using the Variational Principles

The proof of (49) relies on the variational principles (44) and (45). To get an upper bound on real$(I, \Gamma^\epsilon I)$, we take a trial field

$$\mathbf{j}_R(\mathbf{x}) = \left(-\frac{\partial}{\partial y}, \frac{\partial}{\partial x} \right) H_R(x, y) \quad , \tag{51}$$

so that at the boundary

$$H_R(s) = \int^s I_R(s)ds \quad , \tag{52}$$

where s is arclength along $\partial\Omega$. To simplify the exposition let us assume that the excitation current $I(s) = I_R(s) + I_I(s)$ is concentrated at the peripheral nodes of the $R-C$ network, i.e. at the minima of $\max(\rho, \mathcal{C})$ along $\partial\Omega$. Then, H_R and H_I are constant along pieces of the boundary lying between two adjacent peripheral

nodes. Of course, in a real experiment the current excitation is unlikely to satisfy this assumption. Then one must introduce a thin layer near the boundary where the current adjusts from the given I along $\partial\Omega$ to a current concentrated along ridges of minimal ρ or $\mathcal{C}$. The analysis is identical to that of section 2.3 and [10] and shall not be repeated here.

We write the integral in (44) as a sum of integrals over the resistive regions Ω_{ρ_j}, $j = 1, \ldots N_\rho$, the capacitive regions Ω_{C_j}, $j = 1, \ldots N_C$ and the vicinities of interfaces $\mathcal{L}_j$, $j = 1, \ldots N_{\mathcal{L}}$. We analyze these three cases separately.

1. *The resistive region* $\mathbf{x} \in \Omega_{\rho_j}$ for some $j = 1, \ldots N_\rho$, such that $\rho(\mathbf{x}) \gg \mathcal{C}(\mathbf{x})$. In Ω_{ρ_j}, we choose H_R to be a constant away from ridges of minimal ρ. In the vicinity of a ridge of minimal ρ consider coordinates (ξ, η) where ξ is arc length along the ridge. Here the scaled logarithm of ρ is given by

$$S(\xi, \eta) = S(\xi, 0) - \frac{k(\xi)}{2}\eta^2 + \frac{1}{6}\frac{\partial^3 S}{\partial \eta^3}(\xi, 0)\eta^3 + \ldots \quad , \tag{53}$$

where $k(\xi) > 0$ and H_R is chosen as in section 2.2,

$$H_R(\xi, \eta) = -\frac{f_R}{2}\ \mathrm{erf}\ \left(\frac{\eta}{\sqrt{\frac{2\epsilon}{k(\xi)}}}\right) + \text{ constant} \quad , \tag{54}$$

where f_R is the real flux along the ridge. We have

$$\begin{aligned} &\int_{\Omega_{\rho_j}} \left[\rho(\mathbf{x})\left(|\,\mathbf{j}_R(\mathbf{x})\,|^2 - |\,\mathbf{j}_I(\mathbf{x})\,|^2\right) - 2\mathcal{C}(\mathbf{x})\mathbf{j}_R(\mathbf{x})\cdot\mathbf{j}_I(\mathbf{x})\right] d\mathbf{x} \leq \\ &\int_{\Omega_{\rho_j}} \left[(\rho(\mathbf{x}) + \mathcal{C}(\mathbf{x}))\,|\,\mathbf{j}_R(\mathbf{x})\,|^2 - (\rho(\mathbf{x}) - \mathcal{C}(\mathbf{x}))\,|\,\mathbf{j}_I(\mathbf{x})\,|^2\right] d\mathbf{x} \approx \\ &\sum_{\text{ridges in } \Omega_{\rho_j}} \int_{\text{ridge}} \rho(\mathbf{x})\,|\,\mathbf{j}_R(\mathbf{x})\,|^2\, d\mathbf{x} - \int_{\Omega_{\rho_j}} \rho(\mathbf{x})\,|\,\mathbf{j}_I(\mathbf{x})\,|^2\, d\mathbf{x} \quad . \end{aligned} \tag{55}$$

The maximum of (55) is achieved by imaginary currents that satisfy the Euler equation

$$\begin{aligned} \nabla^\perp \cdot \left[\rho_0 e^{-S(\mathbf{x})/\epsilon}\mathbf{j}_I(\mathbf{x})\right] &= 0, \\ \nabla\cdot\mathbf{j}_I(\mathbf{x}) = 0, \quad \mathbf{x} \in \Omega_{\rho_j} \quad . \end{aligned} \tag{56}$$

This equation has been studied in section 2.2 and the result is that $\mathbf{j}_I$ is channeled along ridges of minimal resistance in Ω_{ρ_j}. Moreover,

$$\min_{\mathbf{j}_I} \int_{\Omega_{\rho_j}} \rho(\mathbf{x})\,|\,\mathbf{j}_I(\mathbf{x})\,|^2\, d\mathbf{x} = \min_{f_I} \sum_{\mathbf{x}_S \in \Omega_{\rho_j}} R(\mathbf{x}_S)\left[f_I(\mathbf{x}_S)\right]^2 [1 + o(1)] \quad , \tag{57}$$

where $f_I(\mathbf{x}_S)$ is the net imaginary current through the saddle point $\mathbf{x}_S$ of $\rho(\mathbf{x})$ and $R(\mathbf{x}_S)$ is the effective resistance of the saddle, given by (9), where $\frac{1}{\sigma}$ is replaced by ρ.

Thus, the contribution of Ω_{ρ_j} to the upper bound is

$$\int_{\Omega_{\rho_j}} \left[\rho(\mathbf{x})\left(\mid \mathbf{j}_R(\mathbf{x}) \mid^2 - \mid \mathbf{j}_I(\mathbf{x}) \mid^2\right) - 2\mathcal{C}(\mathbf{x})\mathbf{j}_R(\mathbf{x})\cdot\mathbf{j}_I(\mathbf{x})\right] d\mathbf{x} \leq \max_{f_I} \sum_{\mathbf{x}_S\in\Omega_{\rho_j}} R(\mathbf{x}_S)\left\{[f_R(\mathbf{x}_S)]^2 - [f_I(\mathbf{x}_S)]^2\right\}[1+o(1)] \quad . \tag{58}$$

2. *The capacitive region* $\mathbf{x}\in\Omega_{C_j}$ for some $j=1,\ldots N_C$, such that $\mathcal{C}(\mathbf{x}) \gg \rho(\mathbf{x})$. In Ω_{C_j}, we choose $H_R(\mathbf{x})$ that minimizes $\int_{\Omega_{C_j}} \mathcal{C}_0 e^{-P(\mathbf{x})/\epsilon} \mid \nabla^\perp H_R(\mathbf{x}) \mid^2 d\mathbf{x}$. Clearly, H_R is the solution of

$$\nabla^\perp \cdot \left[\mathcal{C}_0 e^{-P(\mathbf{x})/\epsilon}\nabla^\perp H_R(\mathbf{x})\right] = 0, \quad \text{for } \mathbf{x}\in\Omega_{C_j} \quad . \tag{59}$$

From the results of sections 2.2 and 2.3, we know that, away from ridges of minimal $\mathcal{C}$, $H_R(\mathbf{x})$ is approximately a constant. Take a ridge of minimal $\mathcal{C}$ and consider coordinates (ξ,η) where ξ is arc length along the ridge. In a neighborhood $\mid\eta\mid\leq\delta\ll 1$ such that $\frac{\delta}{\sqrt{\epsilon}}\to\infty$ as $\epsilon\to 0$, we have

$$P(\xi,\eta) = P(\xi,0) - \frac{k(\xi)}{2}\eta^2 + \frac{1}{6}\frac{\partial^3 P}{\partial\eta^3}(\xi,0)\eta^3 + \ldots \quad , \tag{60}$$

where $k(\xi)>0$ and H_R is changing abruptly across the ridge, in such a way that $\mathbf{j}_R = \nabla^\perp H_R = O(\frac{1}{\sqrt{\epsilon}})\hat{\xi}$. The net current along the ridge is $f_R(\xi) = \int_{-\delta}^{\delta} \nabla^\perp H_R(\xi,t)dt$. Note that because of conservation of current $f_R(\xi)$ is either a constant or it changes along the ridge near minima of $\mathcal{C}$. Thus,

$$\int_{\Omega_{C_j}} \mathcal{C}_0 e^{-P(\mathbf{x})/\epsilon} \mid \nabla^\perp H_R(\mathbf{x}) \mid^2 d\mathbf{x} = \min_{f_R} \sum_{\mathbf{x}_S\in\Omega_{C_j}} C(\mathbf{x}_S)\left[f_R(\mathbf{x}_S)\right]^2[1+o(1)] \quad , \tag{61}$$

where $C(\mathbf{x}_S)$ is the effective capacity of the saddle, given by (9) with $\frac{1}{\sigma}$ is replaced by $\mathcal{C}$.

We also study the imaginary current $\mathbf{j}_I = \nabla^\perp H_I(\mathbf{x})$ that maximizes

$$\int_{\Omega_{C_j}} \left[-2\mathcal{C}(\mathbf{x})\nabla^\perp H_R(\mathbf{x})\cdot\nabla^\perp H_I(\mathbf{x}) - \rho(\mathbf{x})\nabla^\perp H_I(\mathbf{x}) \mid^2\right] d\mathbf{x} \quad . \tag{62}$$

The maximization is done over all $H_I(\mathbf{x})$ that satisfy boundary conditions

$$H_I(s) = \int^s \mathbf{j}_I(s)\cdot\mathbf{n}(s)ds \quad , \tag{63}$$

where s is arclength along $\partial\Omega_{C_j}$. The boundary of Ω_{C_j} consists of some interfaces $\mathcal{L}_p$, $p=1,\ldots N_{\mathcal{L}}$ and possibly a piece of $\partial\Omega$. In the resistive regions that are adjacent to Ω_{C_j} the imaginary current is concentrated along ridges of minimal

ρ, as shown in part 1 where we discussed the resistive regions. At the interfaces $\mathcal{L}_p$ these ridges meet the ridges of minimal $\mathcal{C}$ in Ω_{C_j}. Therefore, at the boundary of Ω_{C_j}, the imaginary current is concentrated at the peripheral nodes of the C (static) network and, as given by (63), H_I is a constant along a piece of $\partial\Omega_{C_j}$ that lies between two adjacent peripheral nodes.

We show next that the imaginary current that maximizes (62) is concentrated along the ridges of minimal $\mathcal{C}(\mathbf{x})$, in the interior of Ω_{C_j}. The Euler equation maximizing $\mathbf{j}_I = \nabla^\perp H_I$ satisfies is

$$\nabla^\perp \cdot \left[\rho(\mathbf{x})\nabla^\perp H_I(\mathbf{x}) + \mathcal{C}(\mathbf{x})\nabla^\perp H_R(\mathbf{x})\right] = 0 \ , \tag{64}$$

where the resistance function is of the form

$$\rho(\mathbf{x}) = \mathcal{C}(\mathbf{x})e^{-Q(\mathbf{x})/\epsilon} \ll \mathcal{C}(\mathbf{x}), \qquad \text{where } Q(\mathbf{x}) = S(\mathbf{x}) - P(\mathbf{x}) - \epsilon \log\frac{\rho_0}{\mathcal{C}_0} \ . \tag{65}$$

We construct a function $\tilde{H}_I(\mathbf{x})$ such that

$$\tilde{H}_I(\mathbf{x}) = H_I(\mathbf{x}) \quad \text{ on } \partial\Omega_{C_j} \tag{66}$$

and at $\mathbf{x}$ away from the ridges of minimal $\mathcal{C}(\mathbf{x})$, $\tilde{H}_I(\mathbf{x})$ is constant. In the vicinity of a ridge of minimal $\mathcal{C}$ we take

$$\nabla^\perp \tilde{H}_I(\xi,\eta) = \frac{f_I}{f_R}\nabla^\perp H_R(\xi,\eta) \ . \tag{67}$$

From (65)-(67), we have

$$\begin{aligned}
&\nabla^\perp \left[\rho(\mathbf{x})\nabla^\perp \tilde{H}_I(\mathbf{x}) + \mathcal{C}(\mathbf{x})\nabla^\perp H_R(\mathbf{x})\right] \\
&\qquad = \nabla^\perp \left\{\mathcal{C}(\xi,\eta)\left[1 + \frac{f_I}{f_R}e^{-Q(\xi,\eta)/\epsilon}\right]\nabla^\perp H_R(\xi,\eta)\right\} \\
&\qquad \approx \nabla^\perp \left[\mathcal{C}(\xi,\eta)\nabla^\perp H_R(\xi,\eta)\right] = 0 \ .
\end{aligned} \tag{68}$$

where $e^{-Q(\xi,\eta)/\epsilon} \ll 1$ so that $\rho \ll \mathcal{C}$ holds. Thus, $\tilde{H}_I$ is the approximate solution of the Euler equation (64) and satisfies the same boundary conditions as H_I. By uniqueness of solutions H_I for the elliptic equation (64) we conclude that

$$\nabla^\perp H_I(\xi,\eta) = \frac{f_I}{f_R}\nabla^\perp H_R(\xi,\eta) \ . \tag{69}$$

From (65) and section 2.3 we now have

$$\begin{aligned}
\max_{\nabla^\perp H_I} \int_{\Omega_{C_j}} &\left[\rho(\mathbf{x}) \mid \nabla^\perp H_R(\mathbf{x}) \mid^2 - \rho(\mathbf{x}) \mid \nabla^\perp H_I(\mathbf{x}) \mid^2 \right. \\
&\left. -2C(\mathbf{x})\nabla^\perp H_R(\mathbf{x}) \cdot \nabla^\perp H_I(\mathbf{x})\right] d\mathbf{x} \\
\approx \sum_{\text{ridges in } \Omega_{C_j}} &\int_{\text{ridge}} \left\{\mathcal{C}_0 e^{-P(\xi,\eta)/\epsilon}\left[e^{-Q(\xi,\eta)/\epsilon}\left(\mid \nabla^\perp H_R \mid^2 - \mid \nabla^\perp H_I \mid^2\right)\right.\right.
\end{aligned}$$

$$-2\nabla^\perp H_R \cdot \nabla^\perp H_I \big]\big\}\, d\xi d\eta$$

$$\approx -2 \sum_{\text{ridges in } \Omega_{C_j}} \int_{\text{ridge}} \mathcal{C}_0 e^{-P(\xi,\eta)/\epsilon} \nabla^\perp H_R \cdot \nabla^\perp H_I d\xi d\eta$$

$$\approx \sum_{\text{ridges in } \Omega_{C_j}} \int_{\text{ridge}} \mathcal{C}_0 e^{-P(\xi,0)/\epsilon} \times \frac{f_R(\xi) f_I(\xi) k(\xi)}{2\pi\epsilon} e^{-\frac{k(\xi)\eta^2}{2\epsilon}} d\xi d\eta$$

$$= \sum_{\mathbf{x}_S \in \Omega_{C_j}} C(\mathbf{x}_S) f_R(\mathbf{x}_S) f_I(\mathbf{x}_S) \left[1 + o(1)\right] \ . \tag{70}$$

3. *Resistive-capacitive region.* This is case where $\mathbf{x}$ is in the neighborhood of an interface $\mathcal{L}_j$, $j = 1, \ldots N_{\mathcal{L}}$, where $\rho = \mathcal{C}$. Consider a point $(\xi_{\mathcal{L}}, 0)$ along such an interface, where a ridge of minimal ρ and $\mathcal{C}$ intersects $\mathcal{L}_j$. We define a neighborhood of this point by

$$| \xi - \xi_{\mathcal{L}} | \leq \alpha, \quad | \eta | \leq \delta \ , \tag{71}$$

where (ξ, η) are coordinates along the ridge. Here, α and δ are small and $\frac{\alpha}{\epsilon} \to \infty$ and $\frac{\delta}{\sqrt{\epsilon}} \to \infty$ as $\epsilon \to 0$. Let us assume that there is no saddle point along $\mathcal{L}_j$ and that ρ decreases with ξ. Then $\mathcal{C}$ increases with ξ in such a way that $\rho(\xi_{\mathcal{L}}, 0) = \mathcal{C}(\xi_{\mathcal{L}}, 0)$. We also have the expansions

$$S(\xi, \eta) \approx S(\xi_{\mathcal{L}} - \alpha, 0) + p(\xi - \xi_{\mathcal{L}} + \alpha) - \frac{k(\xi_{\mathcal{L}})}{2}\eta^2 \tag{72}$$

$$P(\xi, \eta) \approx P(\xi_{\mathcal{L}} + \alpha, 0) - q(\xi - \xi_{\mathcal{L}} - \alpha) - \frac{k(\xi_{\mathcal{L}})}{2}\eta^2 \ ,$$

where $p = \frac{\partial S}{\partial \xi}(\xi_{\mathcal{L}} - \alpha, 0) > 0$ and $q = \frac{\partial P}{\partial \xi}(\xi_{\mathcal{L}} + \alpha, 0) > 0$.

In the vicinity of $(\xi_{\mathcal{L}}, 0)$, we choose the trial field

$$H_R(\xi, \eta) \approx -\frac{f_R(\xi_{\mathcal{L}})}{2} \ \text{erf} \ \left(\frac{\eta}{\sqrt{\frac{2\epsilon}{k(\xi_{\mathcal{L}})}}} \right) + \ \text{constant} \ , \tag{73}$$

whereas, away from points such as $(\xi_{\mathcal{L}}, 0)$, H_R is taken to be a constant. Note that our choice of H_R in a thin strip along the interface $\mathcal{L}_j$ agrees with the trial field H_R in the resistive and capacitive regions, separated by $\mathcal{L}_j$. Thus,

$$\nabla^\perp \cdot \left[\mathcal{C}_0 e^{-P(\xi,\eta)/\epsilon} \nabla^\perp H_R(\xi, \eta) \right] \approx \frac{\partial}{\partial \eta} \left[\mathcal{C}_0 e^{-P(\xi,\eta)/\epsilon} \frac{\partial H_R(\xi, \eta)}{\partial \eta} \right] \approx 0 \ . \tag{74}$$

We must calculate

$$\max_{\mathbf{j}_I} \int_{\text{vicinity of } \mathcal{L}_j} \left[-\rho(\mathbf{x}) \ | \mathbf{j}_I(\mathbf{x}) \ |^2 - 2C(\mathbf{x}) \nabla^\perp H_R(\mathbf{x}) \cdot \mathbf{j}_I(\mathbf{x}) \right] d\mathbf{x} \ , \tag{75}$$

where we integrate in a thin strip along the interface $\mathcal{L}_j$. The Euler equation that the maximizing imaginary current $\mathbf{j}_I = \nabla^\perp H_I$ satisfies is

$$\nabla^\perp \cdot \left[\rho(\mathbf{x}) \nabla^\perp H_I(\mathbf{x}) \right] = -\nabla^\perp \cdot \left[\mathcal{C}(\mathbf{x}) \nabla^\perp H_R(\mathbf{x}) \right] \approx 0 \ . \tag{76}$$

Thus, H_I is the solution of the static elliptic equation considered in section 2.2, where σ is replaced by $1/\rho$ and $\nabla^\perp H_I$ is concentrated near minima, such as $(\xi_{\mathcal{L}}, 0)$, of ρ and $\mathcal{C}$ along $\mathcal{L}_j$. From (18) and the assumption that there are no saddle points lying on $\mathcal{L}_j$, we have

$$\int_{\text{vicinity of } \mathcal{L}_j} \rho \mid \nabla^\perp H_I \mid^2 d\mathbf{x} \ll R(\mathbf{x}_S) \left[f_I(\mathbf{x}_S) \right]^2 \quad , \tag{77}$$

where $\mathbf{x}_S$ is the saddle point of ρ that is closest to $(\xi_{\mathcal{L}}, 0)$, along the ridge of minimal resistance.

From (74) we obtain

$$\begin{aligned}
&\int_{\text{vicinity of } \mathcal{L}_j} \mathcal{C} \nabla^\perp H_R \cdot \nabla^\perp H_I d\mathbf{x} \\
&\quad \approx \sum_{(\xi_{\mathcal{L}},0)\in\mathcal{L}_j} \int_{\xi_{\mathcal{L}}-\alpha}^{\xi_{\mathcal{L}}+\alpha} d\xi \int_{-\delta}^{\delta} d\eta \; \mathcal{C}_0 e^{-P(\xi,\eta)/\epsilon} \frac{dH_R(\eta)}{d\eta} \frac{\partial H_I(\xi,\eta)}{\partial \eta} \\
&\quad \approx \int_{\xi_{\mathcal{L}}-\alpha}^{\xi_{\mathcal{L}}+\alpha} d\xi \int_{-\delta}^{\delta} d\eta \frac{\partial}{\partial \eta} \left[H_I(\xi,\eta) \mathcal{C}_0 e^{-P(\xi,\eta)/\epsilon} \frac{dH_R(\eta)}{d\eta} \right] \\
&\quad \approx \int_{\xi_{\mathcal{L}}-\alpha}^{\xi_{\mathcal{L}}+\alpha} \sqrt{\frac{k(\xi_{\mathcal{L}})}{2\pi\epsilon}} f_R(\xi_{\mathcal{L}}) f_I(\xi) \mathcal{C}(\xi_{\mathcal{L}}+\alpha, 0) e^{q(\xi-\xi_{\mathcal{L}}-\alpha)/\epsilon} d\xi \\
&\quad \approx \sqrt{\frac{\epsilon k(\xi_{\mathcal{L}})}{2\pi}} \frac{\mathcal{C}(\xi_{\mathcal{L}}+\alpha, 0)}{q} f_R(\xi_{\mathcal{L}}) f_I(\xi_{\mathcal{L}}) \quad ,
\end{aligned} \tag{78}$$

where $f_I(\xi) = H_I(\xi, -\delta) - H_I(\xi, \delta)$ and we sum over all minima $(\xi_{\mathcal{L}}, 0) \in \mathcal{L}_j$. By assumption, $\mathcal{C}$ decreases with ξ so $\mathcal{C}(\xi_{\mathcal{L}} + \alpha, 0) \leq \mathcal{C}(\mathbf{x}_S)$, where $\mathbf{x}_S$ is the location of the capacitive saddle adjacent to $(\xi_L, 0)$. Thus, (75) is negligible in comparison with the contribution of the saddle points of ρ in regions Ω_{ρ_j}, $j = 1, \ldots N_\rho$, and the saddle points of $\mathcal{C}$ in regions Ω_{C_j}, $j = 1, \ldots N_C$.

We conclude this calculation with the observation that the same result holds if ρ were increasing with ξ instead of decreasing as in (72). However, if $(\xi_{\mathcal{L}}, 0)$ is a saddle point its contribution to the upper bound must be taken into account. The calculation of (75) for $(\xi_{\mathcal{L}}, 0)$ a saddle point is identical to that of (27) in section 2.2 and shall not be repeated here.

We gather all the results in this section to obtain the upper bound

$$\begin{aligned}
\text{real}(I, \Gamma^\epsilon I) \leq \min_{f_R} \max_{f_R} \Bigg\{ &\sum_{j=1}^{N_\rho} \sum_{\mathbf{x}_S \in \Omega_{\rho_j}} R(\mathbf{x}_S) \left[\left(f_R(\mathbf{x}_S) \right)^2 - \left(f_I(\mathbf{x}_S) \right)^2 \right] - \\
&\sum_{j=1}^{N_C} \sum_{\mathbf{x}_S \in \Omega_{C_j}} 2C(\mathbf{x}_S) f_R(\mathbf{x}_S) f_I(\mathbf{x}_S) \Bigg\} \left[1 + o(1) \right] \quad ,
\end{aligned} \tag{79}$$

where the min-max is taken over the fluxes f_R and f_I that satisfy Kirchhoff's nodal law for currents. We get a lower bound on $\text{real}(I, \Gamma^\epsilon I)$, by taking a trial

imaginary current $\mathbf{j}_I$. The calculations are similar to the above and the result is

$$\begin{aligned}\text{real}(I,\Gamma^\epsilon I) \geq \min_{f_R}\ \max_{f_R}\Bigg\{&\sum_{j=1}^{N_\rho}\sum_{\mathbf{x}_S\in\Omega_{\rho_j}} R(\mathbf{x}_S)\left[(f_R(\mathbf{x}_S))^2-(f_I(\mathbf{x}_S))^2\right]- \\ &\sum_{j=1}^{N_C}\sum_{\mathbf{x}_S\in\Omega_{C_j}} 2C(\mathbf{x}_S)f_R(\mathbf{x}_S)f_I(\mathbf{x}_S)\Bigg\}[1+o(1)]\ .\end{aligned} \tag{80}$$

The upper and lower bounds on $\text{real}(I,\Gamma^\epsilon I)$ match asymptotically and we conclude that

$$\begin{aligned}\text{real}(I,\Gamma^\epsilon I) = \min_{f_R}\ \max_{f_R}\Bigg\{&\sum_{j=1}^{N_\rho}\sum_{\mathbf{x}_S\in\Omega_{\rho_j}} R(\mathbf{x}_S)\left[(f_R(\mathbf{x}_S))^2-(f_I(\mathbf{x}_S))^2\right]- \\ &\sum_{j=1}^{N_C}\sum_{\mathbf{x}_S\in\Omega_{C_j}} 2C(\mathbf{x}_S)f_R(\mathbf{x}_S)f_I(\mathbf{x}_S)\Bigg\}[1+o(1)] = \text{real} < \boldsymbol{\mathcal{I}}, \Gamma^{D,\epsilon}\boldsymbol{\mathcal{I}} > [1+o(1)]\ .\end{aligned} \tag{81}$$

A similar calculation leads to

$$\begin{aligned}\text{imag}(I,\Gamma^\epsilon I) = \min_{f_R}\ \max_{f_R}\Bigg\{&\sum_{j=1}^{N_C}\sum_{\mathbf{x}_S\in\Omega_{C_j}} C(\mathbf{x}_S)\left[(f_R(\mathbf{x}_S))^2-(f_I(\mathbf{x}_S))^2\right]+ \\ &\sum_{j=1}^{N_\rho}\sum_{\mathbf{x}_S\in\Omega_{\rho_j}} 2R(\mathbf{x}_S)f_R(\mathbf{x}_S)f_I(\mathbf{x}_S)\Bigg\}[1+o(1)] = \text{imag} < \boldsymbol{\mathcal{I}}, \Gamma^{D,\epsilon}\boldsymbol{\mathcal{I}} > [1+o(1)]\ .\end{aligned} \tag{82}$$

3.3 Remarks on the Variational Principles

It is clear that the min-max variational principles (44) and (45) are essential in the analysis even though they do not seem to have a direct physical meaning, as in the static problem of section 2. In fact, we have

$$(I,\Gamma^\epsilon I) = (I^\star,\Gamma^\epsilon I) + 2i\ (I_I,\Gamma^\epsilon I)\ , \tag{83}$$

where, $\text{real}(I^\star,\Gamma^\epsilon I)$ and $\text{imag}(I^\star,\Gamma^\epsilon I)$ are the power dissipated into heat and the electric energy stored in the system, respectively. Nevertheless, the results (81) and (82) give an approximation of the saddle functionals in (44) and (45) in the asymptotic limit of infinitely high contrast. The current $\mathbf{j}_R + i\ \mathbf{j}_I$ that achieves the min-max in (44) and (45) is the unique solution of equations (42), (43) and, implicitly, of (35). Thus, (81) and (82) show that the current density in a high contrast medium with impedance (39) is approximately given by current flow in an $R-C$ network. We also have

$$\begin{aligned}(I^\star,\Gamma^\epsilon I) &= \int_\Omega \left[\rho_0 e^{-S(\mathbf{x})/\epsilon} + i\ \mathcal{C}_0 e^{-P(\mathbf{x})/\epsilon}\right]\ |\ \mathbf{j}(\mathbf{x})\ |^2\ d\mathbf{x} \\ &= < \boldsymbol{\mathcal{I}}^\star, \Gamma^{D,\epsilon}\boldsymbol{\mathcal{I}} > [1+o(1)]\ .\end{aligned} \tag{84}$$

We have therefore shown that the NtD map Γ^ϵ of the high contrast continuum is assymptotically equivalent to the discrete NtD map of the $R-C$ circuit. This is important for inversions, where the data provide information about the NtD map Γ^ϵ and the asymptotic theory tells us that the first step should be the identification of the asymptotic $R-C$ network.

4 Quasi-Static Approximation: Inductive Approximation

At low frequency the displacement current $i\omega\varepsilon\mathbf{E}$ in (1) can be neglected in conductive media [3, 8]. We consider the transverse electric problem in a simply connected domain $\Omega \subset \mathbb{R}^2$, where $\mathbf{H}(\mathbf{x}) = (0, 0, H(\mathbf{x}))$ and $\mathbf{E}(\mathbf{x}) = (E_1(\mathbf{x}), E_2(\mathbf{x}), 0)$. Equations (1) reduce to

$$\mathbf{E}(\mathbf{x}) = -\frac{1}{\sigma(\mathbf{x})}\nabla^\perp H(\mathbf{x}),$$
$$\nabla^\perp\left[\frac{1}{\sigma(\mathbf{x})}\nabla^\perp H(\mathbf{x})\right] = -i\omega\mu(\mathbf{x})H(\mathbf{x}), \quad \mathbf{x}\in\Omega \ . \tag{85}$$

At the boundary, we specify

$$H(\mathbf{x}) = h(\mathbf{x}) = h_R(\mathbf{x}) + i\ h_I(\mathbf{x}), \quad \mathbf{x}\in\partial\Omega \ , \tag{86}$$

for given h_R and h_I in $\mathrm{H}^{\frac{1}{2}}(\partial\Omega)$. We are interested in high contrast conductive media, where we model the electrical conductivity as in (5). Typically, the variations in magnitude of the magnetic permeability $\mu(\mathbf{x})$ are much smaller than the variations of σ [3]. In fact, $\mu(\mathbf{x})$ is usually assumed to be a constant μ_0, the permeability of free space [3]. We take $\mu(\mathbf{x})$ to be a bounded, continuous function with variations of order one in Ω.

We define the complex map

$$\Upsilon^\epsilon h(\mathbf{x}) = \mathbf{n}(\mathbf{x}) \times \mathbf{E}(\mathbf{x}), \quad \mathbf{x}\in\Omega \ , \tag{87}$$

where $\mathbf{n}(\mathbf{x})$ is the outer normal to the boundary. Given that $\sigma(\mathbf{x})$ is strictly positive and uniformly bounded in Ω, equation (85) with boundary conditions (86) has a unique solution $H(\mathbf{x}) = H_R(\mathbf{x}) + i\ H_I(\mathbf{x})$ (at least in the weak sense), where H_R and H_I are in $\mathrm{H}^1(\Omega)$. Then, the real and imaginary parts of $\Upsilon^\epsilon h$ are in $\mathrm{H}^{-\frac{1}{2}}(\partial\Omega)$ and we define the inner product

$$(h^\star, \Upsilon^\epsilon h) = \int_{\partial\Omega} h^\star(s)\mathbf{e}_3 \cdot [\mathbf{n}(s) \times \mathbf{E}(s)]\, ds \ , \tag{88}$$

where $h^\star$ is the complex conjugate of h and $\mathbf{e}_3$ is the unit vector orthogonal to the plane of Ω. We have

$$(h^\star, \Upsilon^\epsilon h) = \int_{\partial\Omega} [\mathbf{E}(s) \times h^\star(s)\mathbf{e}_3] \cdot \mathbf{n}(s) ds = \int_\Omega \nabla \cdot [\mathbf{E}(\mathbf{x}) \times H^\star(\mathbf{x})\mathbf{e}_3]\, d\mathbf{x} =$$

$$\int_\Omega [H^\star(\mathbf{x})\mathbf{e}_3 \cdot \nabla \times \mathbf{E}(\mathbf{x}) - \mathbf{E}(\mathbf{x}) \cdot \nabla \times H^\star(\mathbf{x})\mathbf{e}_3]\, d\mathbf{x} =$$

$$-\int_\Omega \left[\tfrac{1}{\sigma(\mathbf{x})} \mid \nabla^\perp H(\mathbf{x}) \mid^2 - i\, \omega\mu(\mathbf{x}) \mid H(\mathbf{x}) \mid^2\right] d\mathbf{x} \quad . \tag{89}$$

Thus, the real and imaginary parts of $-(h^\star, \Upsilon^\epsilon h)$ give the power dissipated into heat and the magnetic energy stored in the system, respectively.

We will analyze the complex map (87) in the asymptotic limit $\epsilon \to 0$ and for that we use the min-max variational principles introduced in [8] for quadratic forms of Υ^ϵ. Let us rewrite (85) as an elliptic system of equations

$$\begin{aligned} \nabla^\perp \left[\frac{1}{\sigma_0} e^{S(\mathbf{x})/\epsilon} \nabla^\perp H_R(\mathbf{x})\right] - \omega\mu(\mathbf{x}) H_I(\mathbf{x}) = 0, \\ \nabla^\perp \left[\frac{1}{\sigma_0} e^{S(\mathbf{x})/\epsilon} \nabla^\perp H_I(\mathbf{x})\right] + \omega\mu(\mathbf{x}) H_R(\mathbf{x}) = 0 \quad , \end{aligned} \tag{90}$$

with Dirichlet boundary conditions (86). Equations (90) can be viewed as Euler equations for some real valued functionals. These functionals do not have a direct physical interpretation but do lead to variational principles that characterize the inductive problem. We have

$$\begin{aligned} -\mathrm{real}(h, \Upsilon^\epsilon h) \\ = \min_{H_R|_{\partial\Omega} = h_R} \max_{H_I|_{\partial\Omega} = h_I} \int_\Omega \Big\{ \frac{1}{\sigma_0} e^{S(\mathbf{x})/\epsilon} \left[\mid \nabla^\perp H_R(\mathbf{x}) \mid^2 - \mid \nabla^\perp H_I(\mathbf{x}) \mid^2 \right] \\ + 2\omega\mu(\mathbf{x}) H_R(\mathbf{x}) H_I(\mathbf{x}) \Big\}\, d\mathbf{x} \end{aligned} \tag{91}$$

$$\begin{aligned} \mathrm{imag}(h, \Upsilon^\epsilon h) \\ = \min_{H_R|_{\partial\Omega} = h_R} \max_{H_I|_{\partial\Omega} = h_I} \int_\Omega \Big\{ \omega\mu(\mathbf{x}) \left[H_R(\mathbf{x})\right]^2 - \omega\mu(\mathbf{x}) \left[H_I(\mathbf{x})\right]^2 \\ - 2\frac{1}{\sigma_0} e^{S(\mathbf{x})/\epsilon} \nabla^\perp H_R(\mathbf{x}) \cdot \nabla^\perp H_I(\mathbf{x}) \Big\}\, d\mathbf{x} \end{aligned} \tag{92}$$

In the next section we present an asymptotic analysis of $(h, \Upsilon^\epsilon h)$. We show that the extreemal $\nabla^\perp H_R + i\, \nabla^\perp H_I$ in Ω can be approximated by current flow through a network. We begin with a local asymptotic analysis of (90) after which we solve the global problem by making use of variational principles (91) and (92).

4.1 Local Asymptotic Analysis

We rewrite equation (85) as

$$\nabla H(\mathbf{x}) + \frac{1}{\epsilon}\nabla^{\perp} S(\mathbf{x}) \cdot \nabla^{\perp} H(\mathbf{x}) = -i\omega\mu(\mathbf{x})\sigma(\mathbf{x})H(\mathbf{x}) \tag{93}$$

and observe that the behavior of H in Ω is dictated by the magnitude of $\mu(\mathbf{x})\sigma(\mathbf{x})$ compared to $\frac{1}{\epsilon}$. We assume that equation (93) is in dimensionless form and $\omega = O(1)$. We divide the domain of the solution into "resistive" subdomains Ω_{r_j}, $j = 1, \ldots N_r$, where $\mu(\mathbf{x})\sigma(\mathbf{x}) \ll \frac{1}{\epsilon}$ and "conductive" subdomains Ω_{c_j}, $j = 1, \ldots N_c$, where $\mu(\mathbf{x})\sigma(\mathbf{x}) \gg \frac{1}{\epsilon}$. They are separated by interfaces $\mathcal{L}_j$, $j = 1, \ldots N_{\mathcal{L}}$, where $\mu(\mathbf{x})\sigma(\mathbf{x}) = \frac{1}{\epsilon}$. We study equation (93) in each of these subdomains separately.

1. In *resistive regions* with $\mathbf{x} \in \Omega_{r_j}$ for some $j = 1, \ldots N_r$, such that $\mu(\mathbf{x})\sigma(\mathbf{x}) \ll \frac{1}{\epsilon}$, we show that the current $\nabla^{\perp} H$ behaves essentially like static current in a high contrast medium with conductivity (5). We construct the static network in Ω_{r_j}, as shown in section 2.2, where the nodes are the maxima of σ and the branches go through the saddle points of the conductivity. Take a ridge of maximal σ in Ω_{r_j} as shown in figure 6. We introduce the curvilinear coordinates (ξ, η), where ξ is arclength along the ridge and η is orthogonal to it. We define a vicinity of the ridge by

$$| \eta | \leq \delta \ll 1 \ , \tag{94}$$

where $\frac{\delta}{\sqrt{\epsilon}} \to \infty$ as $\epsilon \to 0$. In this region the scaled logarithm of σ is given by

$$S(\xi, \eta) = S(\xi, 0) + \frac{k(\xi)}{2}\eta^2 + \frac{1}{6}\frac{\partial^3 S}{\partial \eta^3}(\xi, 0)\eta^3 + \ldots \ , \tag{95}$$

where $k(\xi) > 0$. Suppose that at the point ξ_M of maximal conductivity along the ridge, $\mu(\xi_M, 0)\sigma(\xi_M, 0) = \frac{1}{\epsilon^{1-\alpha}} \ll \frac{1}{\epsilon}$, for some $\alpha > 0$. Then,

$$\mu(\xi, 0)\sigma(\xi, 0) = \frac{1}{\epsilon^{1-\alpha}}\frac{\mu(\xi, 0)}{\mu(\xi_M, 0)}\exp\left[\frac{S(\xi, 0) - S(\xi_M, 0)}{\epsilon}\right] \leq \frac{1}{\epsilon^{1-\alpha}} \ . \tag{96}$$

Now we write (93) in terms of η and ξ, for points in the vicinity (94) of a ridge of maximal conductivity. Take a point $\mathbf{x}(\xi)$ along the ridge, as shown in figure 6. Let $\hat{\xi}$ and $\hat{\eta}$ denote the unit tangent and normal to the ridge, respectively. In the vicinity (94), we have

$$\mathbf{x} = \mathbf{x}(\xi) + \eta\hat{\eta} \tag{97}$$

and so,

$$d\mathbf{x} = \left[\hat{\xi} + \eta\hat{\eta}'\right] d\xi + \hat{\eta} d\eta, \quad \text{where } \hat{\eta}' = \gamma(\xi)\hat{\xi} \text{ and } \gamma(\xi) = O(1) \ . \tag{98}$$

Then,

$$\begin{aligned} \left(\frac{\partial}{\partial x}, \frac{\partial}{\partial y}\right) H &\approx \frac{\partial H}{\partial \xi} + \frac{\partial H}{\partial \eta}, \\ \Delta H &\approx \frac{\partial^2 H}{\partial \eta^2} + \gamma(\xi)\frac{\partial H}{\partial \eta} + \frac{\partial^2 H}{\partial \xi^2} \end{aligned} \tag{99}$$

and, with scaling $\eta = \sqrt{\epsilon} z$, equation (93) becomes

$$\frac{\partial^2 H}{\partial z^2} + \sqrt{\epsilon}\gamma(\xi)\frac{\partial H}{\partial z} + \epsilon\frac{\partial^2 H}{\partial \xi^2} + k(\xi) z \frac{\partial H}{\partial z} + \left[S'(\xi,0) + \epsilon z^2 k'(\xi)\right]\frac{\partial H}{\partial \xi}$$
$$\approx \omega \epsilon^{\alpha} \frac{\mu(\xi,0)}{\mu(\xi_M,0)} e^{\frac{S(\xi,0)-S(\xi_M,0)}{\epsilon} - \frac{k(\xi)z^2}{2}} H \quad . \tag{100}$$

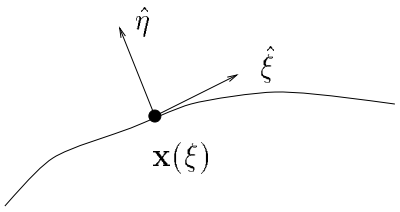

Fig. 6. Ridge of maximal $\sigma(\mathbf{x})$ and curvilinear coordinates (ξ, η).

Thus, $H(\xi,\eta) \approx H_0(\xi,\eta)$, where H_0 solves

$$\frac{\partial^2 H_0}{\partial z^2} + k(\xi) z \frac{\partial H_0}{\partial z} + S'(\xi,0)\frac{\partial H_0}{\partial \xi} = 0. \tag{101}$$

This is, to leading order, the static elliptic equation

$$\nabla^{\perp}\left\{\frac{1}{\sigma_0} e^{S(\xi,\eta)/\epsilon}\nabla^{\perp}\left[H_0(\xi, \frac{\eta}{\sqrt{\epsilon}}) + O(\sqrt{\epsilon})\right]\right\} = 0 \quad , \tag{102}$$

studied in section 2.3. As we move away from the ridge of maximal conductivity, the coefficient of H on the right hand side of equation (93) becomes

$$\begin{aligned}\mu(\mathbf{x})\sigma(\mathbf{x}) &= \frac{1}{\epsilon^{1-\alpha}}\frac{\mu(\mathbf{x})}{\mu(\xi_M,0)}\exp\left[\frac{S(\mathbf{x}) - S(\xi_M,0)}{\epsilon}\right] \\ &= O\left(\frac{1}{\epsilon^{1-\alpha}}\exp\left[\frac{S(\mathbf{x}) - S(\xi_M,0)}{\epsilon}\right]\right) \quad . \end{aligned} \tag{103}$$

Here, $S(\mathbf{x}) < S(\xi_M,0)$ and $\sigma(\mathbf{x})$ is much smaller than $\sigma(\xi_M,0)$, the maximal conductivity along the ridge of maximal σ. Indeed, by assumption $S(\mathbf{x})$ is a smooth function with derivatives of order one, so outside the vicinity (94) of the ridge of maximal σ we have $|S(\mathbf{x}) - S(\xi_M,0)| \geq O(\sqrt{\epsilon})$ and $\mu(\mathbf{x})\sigma(\mathbf{x}) \ll 1$. Thus, $H(\mathbf{x}) \approx \tilde{H}(\mathbf{x})$, which is the solution of static equation

$$\nabla^{\perp}\left[\frac{1}{\sigma_0} e^{S(\mathbf{x})/\epsilon}\nabla^{\perp}\tilde{H}(\mathbf{x})\right] = 0 \quad .$$

As shown in section 2.3, $\nabla^\perp H(\mathbf{x})$ for $\mathbf{x} \in \Omega_{r_j}$, $j = 1, \ldots N_r$ can be approximated by current flowing through a resistor network with its topology defined uniquely by the ridges of maximal σ contained in Ω_{r_j}.

2. In *conductive regions* $\mathbf{x} \in \Omega_{c_j}$ for some $j = 1, \ldots N_c$, so that $\mu(\mathbf{x})\sigma(\mathbf{x}) \gg \frac{1}{\epsilon}$, we see from equation (93), that $H \approx 0$ or, equivalently, the highly conductive regions Ω_{c_j} expell the magnetic and electric fields. This is a well known phenomenon, found in the literature under such names as skin depth penetration and the Meissner effect [31,49]. Of course, the magnetic field H in Ω_{c_j} has to match the field in the nearby resistive regions Ω_{r_j}. The matching is done in the vicinity of interfaces $\mathcal{L}_j$, $j = 1, \ldots N_{\mathcal{L}}$, where $\mu(\mathbf{x})\sigma(\mathbf{x}) = \frac{1}{\epsilon}$.

3. At *interfaces* $\mathcal{L}_j$ we introduce curvilinear coordinates (ξ, η), as shown in figure 7. We define a neighborhood of $\mathcal{L}_j$ by

$$| \eta | \leq \delta \ll 1 \ , \tag{104}$$

where $\frac{\delta}{\epsilon} \to \infty$ as $\epsilon \to 0$. Here, the scaled logarithm of σ is given by

$$S(\xi, \eta) = S(\xi, 0) - \lambda(\xi)\eta + \frac{1}{2}\frac{\partial^2 S}{\partial \eta^2}(\xi, 0)\eta^2 + \ldots \ , \tag{105}$$

where $\lambda(\xi) > 0$, so that σ increases with η. We also have that

$$\mu(\xi, 0)\frac{1}{\sigma_0}e^{S(\xi,0)/\epsilon} = \frac{1}{\epsilon} \ . \tag{106}$$

After a calculation similar to that in part 1 above, leading to equations (99), we have

$$\frac{\partial^2 H}{\partial \eta^2} - \gamma(\xi)\frac{\partial H}{\partial \eta} + \frac{\partial^2 H}{\partial \xi^2} - \lambda(\xi)\epsilon\frac{\partial H}{\partial \eta} + \frac{1}{\epsilon}\left[S'(\xi, 0) - \lambda'(\xi)\eta\right]\frac{\partial H}{\partial \xi} + i\frac{\omega}{\epsilon}e^{\frac{\lambda(\xi)\eta}{\epsilon}}H = 0 \ . \tag{107}$$

We introduce the stretching $\eta = \sqrt{\epsilon}z$ and look for a solution H of the form

$$H(\xi, z) \approx \exp\left[\frac{P(\xi, z)}{\sqrt{\epsilon}}\right] \ . \tag{108}$$

To leading order $\frac{1}{\epsilon^2}$ we have

$$\left(\frac{\partial P}{\partial z}\right)^2 - \lambda(\xi)\frac{\partial P}{\partial z} + i\ \omega\epsilon e^{\frac{\lambda(\xi)z}{\sqrt{\epsilon}}} = 0 \tag{109}$$

and

$$P(\xi, z) = P(\xi, 0) + \frac{1}{2}\lambda(\xi)z \pm \frac{1}{2}\lambda(\xi)\int_0^z \sqrt{1 - 4i\frac{\omega\epsilon}{\lambda^2(\xi)}e^{\frac{\lambda(\xi)t}{\sqrt{\epsilon}}}}\,dt \ . \tag{110}$$

From (110) we note that $H(\xi, z)$ to be bounded we must discard the solution with the plus sign in front of the integral. Thus, from (108) and (110) we have

$$H(\xi, \eta) \approx H(\xi, 0)\exp\left[\frac{\lambda(\xi)\eta}{2\epsilon} - \frac{\lambda(\xi)}{2}\int_0^{\frac{\eta}{\epsilon}} \sqrt{1 - 4i\frac{\omega\epsilon}{\lambda^2(\xi)}e^{\lambda(\xi)t}}\,dt\right] \ . \tag{111}$$

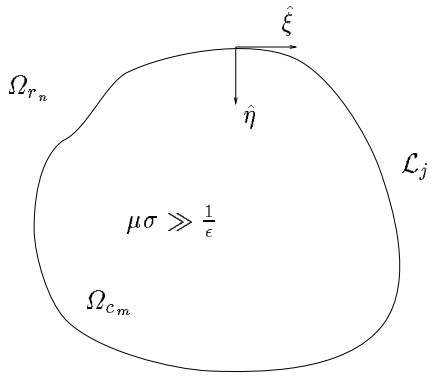

Fig. 7. Highly conductive region Ω_{c_m} separated from the resistive region Ω_{r_n} by interface $\mathcal{L}_j$.

From (111) we see that for $\eta < O(\epsilon)$, $H(\xi, \eta) \approx H(\xi, 0)$ and the magnetic field matches the field in the adjacent resistive region. However, for $\eta > O(\epsilon)$ (111) decays exponentially towards zero, the value of the magnetic field inside the conductive region. Because of the exponential decay of (111) there is a strong current $\nabla^{\perp} H(\xi, \eta) \approx -\frac{\partial H}{\partial \eta}\hat{\xi}$, along the interface $\mathcal{L}_j$.

4.2 Global Asymptotic Approximation

The local analysis of section 4.1 shows that $\nabla^{\perp} H$ is channeled in Ω either along ridges of maximal σ or along interfaces $\mathcal{L}_j$, $j = 1, \ldots N_{\mathcal{L}}$, that separate resistive subdomains Ω_{r_j}, $j = 1, \ldots N_r$ from highly conductive ones, Ω_{c_j}, $j = 1, \ldots N_c$. In fact, $\nabla^{\perp} H$ is like current through a network. First we establish the topology of the network, as follows.

We construct the static resistor network in the whole domain Ω as explained in section 2.2. Then we identify the highly conductive regions Ω_{c_j}, $j = 1, \ldots N_c$. We discard the pieces of the static network that fall inside Ω_{c_j} and we connect the loose ends through "wires" along the interfaces $\mathcal{L}_j$, $j = 1, \ldots N_{\mathcal{L}}$. The topology of the network is now uniquely defined for any σ of the form (5).

In figures 8 and 9 we illustrate the construction of the asymptotic network for an example of conductivity $\sigma_0 e^{-S(\mathbf{x})/\epsilon}$ with five maxima denoted by $\circ$, four minima denoted by $\bullet$ and saddle points counted from 1 to 4, respectively. Inside the dotted closed curve in figure 8 we assume that $\mu\sigma \gg \frac{1}{\epsilon}$. In the remainder of the domain $\mu\sigma \ll \frac{1}{\epsilon}$. The global network is shown in figure 9, where the assignment of impedances $Z_1, \ldots Z_8$ is discussed in the next section. The branches (e, f), (f, g), (g, h) and (h, e) are pieces of the dotted interface in figure 8 where $\mu\sigma = \frac{1}{\epsilon}$.

We will now analyze the quadratic forms $(h, \Upsilon^{\epsilon} h)$ up to $o(1)$ by making use of the variational principles (91) and (92). For simplicity we assume that h_R and h_I in (86) are constant along pieces of $\partial\Omega$ that lie between adjacent peripheral

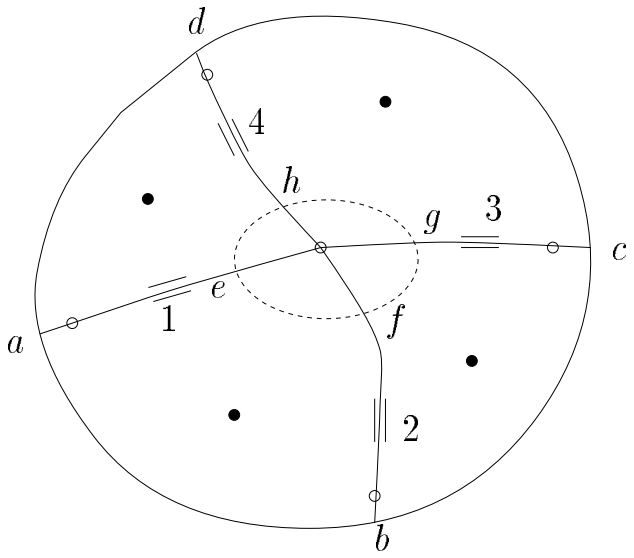

Fig. 8. Example of $\sigma(\mathbf{x}) = \sigma_0 e^{-S(\mathbf{x})/\epsilon}$. The topology of the static resistor network is shown with full line. Inside the dotted curve, $\mu\sigma \gg \frac{1}{\epsilon}$. In the remainder of the domain, $\mu\sigma \ll \frac{1}{\epsilon}$.

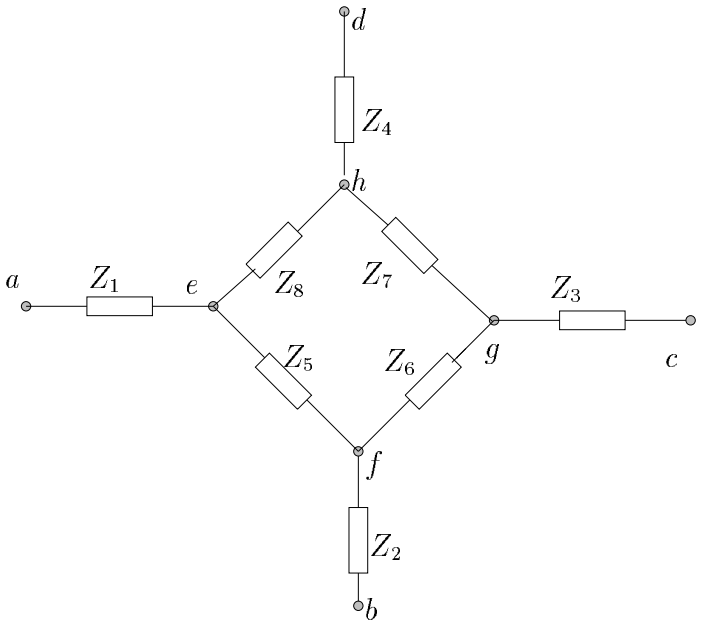

Fig. 9. A possible global network

nodes of the network in Ω. Equivalently, in the direction normal to the boundary, currents $\nabla^\perp H_R$ and $\nabla^\perp H_I$ are concentrated around the peripheral nodes of the network. In a general situation we have h_R and h_I arbitrary functions in $\mathrm{H}^{\frac{1}{2}}(\partial\Omega)$ and, in thin boundary layers, $\nabla^\perp H_R$ and $\nabla^\perp H_I$ adjust to currents concentrated through the asymptotic network. The analysis is identical to that of section 2.3 and [10] and shall not be repeated here.

We begin with the calculation of an upper bound on $-\mathrm{real}(h, \Upsilon^\epsilon h)$, obtained with a trial field H_R chosen as follows. For $\mathbf{x} \in \Omega_{r_j}$ for some $j = 1, \ldots N_r$, such that $\mu(\mathbf{x})\sigma(\mathbf{x}) \ll \frac{1}{\epsilon}$ we take H_R to be a constant away from ridges of maximal σ. In the vicinity of a ridge of maximal σ consider coordinates (ξ, η) where ξ is arc length along the ridge. Here, the scaled logarithm of σ is given by

$$S(\xi, \eta) = S(\xi, 0) + \frac{k(\xi)}{2}\eta^2 + \frac{1}{6}\frac{\partial^3 S}{\partial \eta^3}(\xi, 0)\eta^3 + \ldots \ , \tag{112}$$

where $k(\xi) > 0$ and H_R is chosen as

$$H_R(\xi, \eta) = -\frac{f_R}{2} \ \mathrm{erf} \ \left(\frac{\eta}{\sqrt{\frac{2\epsilon}{k(\xi)}}} \right) + \ \mathrm{constant} \ , \tag{113}$$

where f_R is the real flux along the ridge. By conservation of current, f_R is a constant along the ridge or changes only near maxima of σ. For $\mathbf{x} \in \Omega_{c_j}$ for some $j = 1, \ldots N_c$, such that $\mu(\mathbf{x})\sigma(\mathbf{x}) \gg \frac{1}{\epsilon}$, we take $H_R = 0$.

For $\mathbf{x} \in \mathcal{L}_j$, $j = 1, \ldots N_{\mathcal{L}}$, so that $\mu(\mathbf{x})\sigma(\mathbf{x}) = \frac{1}{\epsilon}$ we introduce curvilinear coordinates (ξ, η) as in section 4.1, part 2 and a vicinity of $\mathcal{L}_j$ as in (104). In this vicinity the scaled logarithm of σ is given by

$$S(\xi, \eta) = S(\xi, 0) - \lambda(\xi)\eta + \frac{1}{2}\frac{\partial^2 S}{\partial \eta^2}(\xi, 0)\eta^2 + \ldots \tag{114}$$

and we take $H_R(\xi, \eta)$ to be

$$\begin{aligned} H_R(\xi, \eta) \ = \mathrm{real} \Big\{ \Big[H_R(\xi, 0) + i\tilde{H}_I(\xi, 0) \Big] \\ \exp\left[\frac{\lambda(\xi)\eta}{2\epsilon} - \frac{\lambda(\xi)}{2} \int_0^{\frac{\eta}{\epsilon}} \sqrt{1 - 4i\frac{\omega\epsilon}{\lambda^2(\xi)} e^{\lambda(\xi)t}}\, dt \right] \Big\} \end{aligned} \tag{115}$$

Here, $\tilde{H}_I = O(1)$, is a function of arclength along the interface, to be specified later. Note that for any $\tilde{H}_I$, when $\eta \leq O(\epsilon)$ equation (115) gives $H_R(\xi, \eta) \approx H_R(\xi, 0)$.

For $\eta \gg \epsilon$, $H_R(\xi, \eta) \approx 0$. Thus, the trial field H_R is continuous, as required, throughout Ω for an arbitrary $\tilde{H}_I$. In figure 10 we illustrate our choice of trial field H_R, for the example of figure 8.

We now write the integral in (91) as a sum of integrals over the resistive regions Ω_{r_j}, $j = 1, \ldots N_r$, the conductive regions Ω_{c_j}, $j = 1, \ldots N_c$ and the vicinities of interfaces $\mathcal{L}_j$, $j = 1, \ldots N_{\mathcal{L}}$. We obtain an upper bound on $-\mathrm{real}(h, \Upsilon^\epsilon h)$

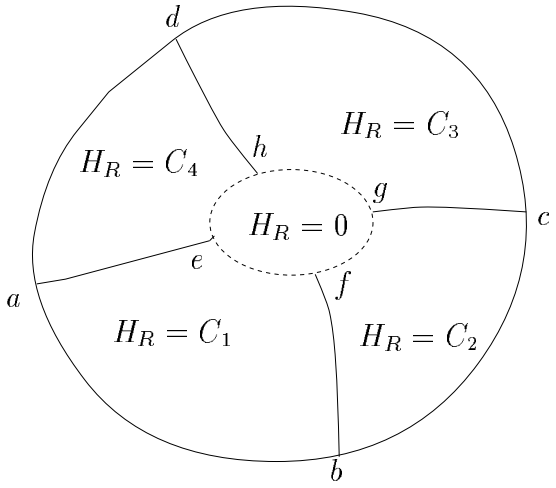

Fig. 10. Trial field H_R for the upper bound on $-\text{real}(h, \Upsilon^\epsilon h)$. In the resistive region, where $\mu\sigma \ll \frac{1}{\epsilon}$ and away from ridges of maximal σ we take H_R to be a constant. Across ridges of maximal σ, H_R is chosen as in (113). In the conductive region, where $\mu\sigma \gg \frac{1}{\epsilon}$, $H_R = 0$.

by using the trial field H_R defined above and maximizing the integral over each subdomain in Ω.

1. In resistive regions $\mathbf{x} \in \Omega_{r_j}$ for some $j = 1, \ldots N_r$, so that $\mu(\mathbf{x})\sigma(\mathbf{x}) \ll \frac{1}{\epsilon}$, we wish to calculate

$$\max_{H_I} \int_{\Omega_{r_j}} \left\{ \frac{1}{\sigma_0} e^{S(\mathbf{x})/\epsilon} \left[\mid \nabla^\perp H_R(\mathbf{x}) \mid^2 - \mid \nabla^\perp H_I(\mathbf{x}) \mid^2 \right] + 2\omega\mu(\mathbf{x}) H_R(\mathbf{x}) H_I(\mathbf{x}) \right\} \ . \tag{116}$$

The maximum is achieved by fields H_I that satisfy

$$\Delta H_I(\mathbf{x}) + \frac{1}{\epsilon} \nabla^\perp S(\mathbf{x}) \cdot \nabla^\perp H_I(\mathbf{x}) = -\omega\mu(\mathbf{x})\sigma(\mathbf{x}) H_R(\mathbf{x}) \ . \tag{117}$$

Clearly, this is very similar to equation (93), considered in section 4.1, part 1. We can state the result: $H_I(\mathbf{x}) \approx \tilde{H}_I(\mathbf{x})$, where

$$\nabla^\perp \left[\frac{1}{\sigma_0} e^{S(\mathbf{x})/\epsilon} \nabla^\perp \tilde{H}_I(\mathbf{x}) \right] = 0 \ . \tag{118}$$

Suppose that the ridges of maximal σ divide Ω_{r_j} into regions $\mathcal{D}_l, l = 1, \ldots n_{r_j}$. In such a region, say $\mathcal{D}_l$, our trial field is a constant, say $H_R = C_l$. From (118) and the results of sections 2.2 and 2.3, $H_I \approx \tilde{H}_I = D_l$, where D_l is a constant. Near a ridge of maximal σ, both H_R and $\tilde{H}_I$ change very fast and we have strong currents $\nabla^\perp H_R$ and $\nabla^\perp \tilde{H}_I$ of order $1/\sqrt{\epsilon}$ along the ridge. From section 2.2 we

also have

$$\int_{\Omega_{r_j}} \frac{1}{\sigma_0} e^{S(\mathbf{x})/\epsilon} \mid \nabla^{\perp} H_R(\mathbf{x}) \mid^2 d\mathbf{x} = \sum_{\mathbf{x}_S \in \Omega_{r_j}} R(\mathbf{x}_S) \left[f_R(\mathbf{x}_S) \right]^2 [1 + o(1)] \qquad (119)$$

and

$$\int_{\Omega_{r_j}} \frac{1}{\sigma_0} e^{S(\mathbf{x})/\epsilon} \mid \nabla^{\perp} \tilde{H}_I(\mathbf{x}) \mid^2 d\mathbf{x} = \sum_{\mathbf{x}_S \in \Omega_{r_j}} R(\mathbf{x}_S) \left[f_I(\mathbf{x}_S) \right]^2 [1 + o(1)] \quad , \qquad (120)$$

where $R(\mathbf{x}_S)$ is the effective resistance of the saddle point $\mathbf{x}_S$ and $f_R(\mathbf{x}_S)$ and $f_I(\mathbf{x}_S)$ are the real and imaginary fluxes through it, respectively. Note that f_R and f_I are completely determined by C_l and D_l, the values of H_R and $\tilde{H}_I$ in the regions $\mathcal{D}_l$, $l = 1, \ldots n_{r_j}$, of diffuse flow.

Collecting the contributions from the region Ω_{r_j} to the upper bound for $-\text{real}(h, \Upsilon^{\epsilon} h)$ it becomes

$$\max_{D_l} \left\{ \sum_{\mathbf{x}_S \in \Omega_{r_j}} R(\mathbf{x}_S) \left[\left(f_R(\mathbf{x}_S) \right)^2 - \left(f_I(\mathbf{x}_S) \right)^2 \right] + 2\omega \sum_{l=1}^{n_{r_j}} C_l D_l \int_{\mathcal{D}_l} \mu(\mathbf{x}) d\mathbf{x} \right\} [1 + o(1)] \quad . \qquad (121)$$

2. In transition regions $\mathbf{x} \in \mathcal{L}_j$ for some $j = 1, \ldots N_r$, such that $\mu(\mathbf{x})\sigma(\mathbf{x}) = \frac{1}{\epsilon}$ we calculate

$$\max_{H_I} \int d\xi \int_{-\delta}^{\delta} d\eta \left\{ \frac{1}{\sigma_0} e^{S(\xi,\eta)/\epsilon} \left[\mid \nabla^{\perp} H_R(\xi,\eta) \mid^2 - \mid \nabla^{\perp} H_I(\xi,\eta) \mid^2 \right] \right.$$
$$\left. + 2\omega\mu(\xi,\eta) H_R(\xi,\eta) H_I(\xi,\eta) \right\} \quad , \qquad (122)$$

where we integrate in the vicinity (104) defined in section 4.1, part 2, such that $\omega\mu(\xi,\eta) \approx \mu(\xi,0)$. The maximum is achieved by fields H_I that satisfy

$$\Delta H_I(\xi,\eta) + \frac{1}{\epsilon} \nabla^{\perp} S(\xi,\eta) \cdot \nabla^{\perp} H_I(\xi,\eta)$$
$$\approx -\omega\mu(\xi,0)\sigma(\xi,\eta) \text{real} \left\{ \left[H_R(\xi,0) + i\tilde{H}_I(\xi,0) \right] \times \right.$$
$$\left. \exp\left[\frac{\lambda(\xi)\eta}{2\epsilon} - \frac{\lambda(\xi)}{2} \int_0^{\frac{\eta}{\epsilon}} \sqrt{1 - 4i\frac{\omega\epsilon}{\lambda^2(\xi)} e^{\lambda(\xi)t}} dt \right] \right\} \qquad (123)$$

Recall that any $\tilde{H}_I(\xi, 0)$ in (115) gives an acceptable trial field H_R. We are therefore free to choose $\tilde{H}_I$ as the solution of equation (118) and since (123) has been solved in section 4.1, part 2, we have

$$H_I(\xi,\eta) \approx \text{imag} \left\{ \left[H_R(\xi,0) + i\tilde{H}_I(\xi,0) \right] \right.$$
$$\left. \exp\left[\frac{\lambda(\xi)\eta}{2\epsilon} - \frac{\lambda(\xi)}{2} \int_0^{\frac{\eta}{\epsilon}} \sqrt{1 - 4i\frac{\omega\epsilon}{\lambda^2(\xi)} e^{\lambda(\xi)t}} dt \right] \right\} \qquad (124)$$

Note that, for $\eta \leq O(\epsilon)$, we have the correct matching of the imaginary field, since $H_I(\xi,\eta) \approx \tilde{H}_I(\xi,0)$. For $\eta \gg O(\epsilon)$, $H_I \approx 0$.

Because of the rapid variation with η of both H_R and H_I we have a strong current, of order $1/\sqrt{\epsilon}$, concentrated near the interface $\mathcal{L}_j$ and given by

$$\begin{aligned}
&\nabla^\perp \left[H_R(\xi,\eta) + i\ H_I(\xi,\eta)\right] \\
&\quad \approx -\frac{\partial}{\partial \eta}\left[H_R(\xi,\eta) + i\ H_I(\xi,\eta)\right]\hat{\xi} \\
&\quad = \left[H_R(\xi,0) + i\tilde{H}_I(\xi,0)\right]\frac{\lambda(\xi)}{\epsilon}\left[\sqrt{1-4i\ \frac{\omega\epsilon}{\lambda^2(\xi)}e^{\frac{\lambda(\xi)\eta}{\epsilon}}} - 1\right] \\
&\quad \times \exp\left[\frac{\lambda(\xi)\eta}{2\epsilon} - \frac{\lambda(\xi)}{2}\int_0^{\frac{\eta}{\epsilon}}\sqrt{1-4i\frac{\omega\epsilon}{\lambda^2(\xi)}e^{\lambda(\xi)t}}dt\right]\hat{\xi}\ . \qquad (125)
\end{aligned}$$

Here $\hat{\xi}$ is the unit vector tangential to $\mathcal{L}_j$. Thus, (122) becomes

$$\begin{aligned}
&\mathrm{real}\int d\xi \frac{\lambda^2(\xi)\left[H_R(\xi,0) + i\ \tilde{H}_I(\xi,0)\right]^2}{4\epsilon^2\sigma(\xi,0)}\int_{-\delta}^{\delta}d\eta\left[\sqrt{1-4i\ \frac{\omega\epsilon}{\lambda^2(\xi)}e^{\frac{\lambda(\xi)\eta}{\epsilon}}} - 1\right]^2 \\
&\qquad \cdot e^{-\lambda(\xi)\int_0^{\frac{\eta}{\epsilon}}\sqrt{1-4i\frac{\omega\epsilon}{\lambda^2(\xi)}e^{\lambda(\xi)t}}dt} \\
&+\mathrm{imag}\int d\xi\omega\mu(\xi,0)\left[H_R(\xi,0) + i\ \tilde{H}_I(\xi,0)\right]^2\int_{-\delta}^{\delta}d\eta \\
&\qquad \cdot e^{\frac{\lambda(\xi)\eta}{\epsilon}-\lambda(\xi)\int_0^{\frac{\eta}{\epsilon}}\sqrt{1-4i\frac{\omega\epsilon}{\lambda^2(\xi)}e^{\lambda(\xi)t}}dt}\ . \qquad (126)
\end{aligned}$$

Note that the last term in (126) is of order $\delta\omega\int\mu(\xi,0)d\xi$ and is much smaller than (121). We are left with

$$\mathrm{real}\int d\xi\frac{\lambda^2(\xi)\left[H_R(\xi,0) + i\ \tilde{H}_I(\xi,0)\right]^2}{4\epsilon\sigma(\xi,0)}\mathcal{F}(\xi)\ , \qquad (127)$$

where with the change of variable $s = \frac{\eta}{\epsilon}$, $|\eta| < \delta$ and $\frac{\delta}{\epsilon} \to \infty$, we have

$$\mathcal{F}(\xi) = \int_{-\infty}^{\infty}ds\left[\sqrt{1-4i\ \frac{\omega\epsilon}{\lambda^2(\xi)}e^{\lambda(\xi)s}} - 1\right]^2 e^{-\lambda(\xi)\int_0^s\sqrt{1-4i\frac{\omega\epsilon}{\lambda^2(\xi)}e^{\lambda(\xi)t}}dt}\ . \qquad (128)$$

The integrand in (128) is a smooth complex function with compact support and $\mathcal{F}(\xi)$ is an absolutely convergent integral. We cannot evaluate explicitly $\mathcal{F}(\xi)$ but we can easily do so numerically. It has the form

$$\mathcal{F}(\xi) = -\frac{\epsilon^2\omega^2}{\lambda^5(\xi)}\mathcal{G}_1(\xi) - i\frac{\epsilon\omega}{\lambda^3(\xi)}\mathcal{G}_2(\xi)\ , \qquad (129)$$

where $\mathcal{G}_1(\xi)$ and $\mathcal{G}_2(\xi)$ are two positive functions of order one that are independent of ϵ, ω and $\lambda(\xi)$. Thus, the contribution of the interface $\mathcal{L}_j$ to the upper bound on $-\text{real}(h, \Upsilon^\epsilon h)$ is

$$2\omega \int H_R(\xi,0)\tilde{H}_I(\xi,0)\frac{\mathcal{G}_2(\xi)}{\lambda(\xi)\sigma(\xi,0)}d\xi \quad . \tag{130}$$

Note also that along $\mathcal{L}_j$, $H_R(\xi,0)$ and $\tilde{H}_I(\xi,0)$ are approximately constant between two adjacent points of intersection of the interface and the ridges of maximal σ (see for example figure 10).

The upper bound for $-\text{real}(h, \Upsilon^\epsilon h)$, follows from (121) and (130) and is

$$-\text{real}(h,\Upsilon^\epsilon h) \leq \min_{C_l}\max_{D_l}\sum_{j=1}^{N_r}\left\{\sum_{\mathbf{x}_S\in\Omega_{r_j}} R(\mathbf{x}_S)\left[(f_R(\mathbf{x}_S))^2-(f_I(\mathbf{x}_S))^2\right]\right.$$
$$\left.+2\omega\sum_{l=1}^{n_{r_j}} C_l D_l L_l\right\}[1+o(1)] \quad , \tag{131}$$

where L_l is the inductance associated with region $\mathcal{D}_l$, $l = 1, \ldots n_{r_j}$, of diffuse flow. Suppose that the boundary of $\mathcal{D}_l$ consists only of ridges of maximal σ lying in the resistive region Ω_{r_j}. Then,

$$L_l = \int_{\mathcal{D}_l} \mu(\mathbf{x})d\mathbf{x} \quad . \tag{132}$$

If part of the boundary of $\mathcal{D}_l$ consists of a piece of interface $\mathcal{L}_k$ then the inductance L_l is given by

$$L_l = \int_{\mathcal{D}_l}\mu(\mathbf{x})d\mathbf{x} + 2\omega\int_{\xi_1}^{\xi_2}\frac{\mathcal{G}_2(\xi)}{\lambda(\xi)\sigma(\xi,0)}d\xi \quad ,$$

where ξ_1 and ξ_2 are the endpoints of the piece of $\mathcal{L}_k$ that bounds $\mathcal{D}_l$. Note that here, $\frac{1}{\sigma(\xi,0)} = \epsilon\mu(\xi,0)$ and since μ has variations of order one equation (132) still holds, approximately.

We conclude our calculation of the upper bound (131) with the observation that we take the min-max over the real and imaginary constant values of the magnetic field, in regions $\mathcal{D}_l$ of diffuse flow. This min-max is constrained by the boundary conditions imposed on H_R and H_I, so that C_l and D_l are prescribed in regions $\mathcal{D}_l$ that touch $\partial\Omega$. Then, from the first order optimality condition in (131), we obtain a full-rank, linear system of equations which determines uniquely the upper bound for $-\text{real}(h, \Upsilon^\epsilon h)$.

The calculation of a lower bound for $-\text{real}(h, \Upsilon^\epsilon h)$ starts by choosing and imaginary trial field H_I. The technique is very similar to the one above and the resulting lower bound matches asymptotically the upper bound (131) so that

$$-\text{real}(h,\Upsilon^\epsilon h) = \min_{C_l}\max_{D_l}\sum_{j=1}^{N_r}\left\{\sum_{\mathbf{x}_S\in\Omega_{r_j}} R(\mathbf{x}_S)\left[(f_R(\mathbf{x}_S))^2-(f_I(\mathbf{x}_S))^2\right]\right.$$

$$+2\omega\sum_{l=1}^{n_{r_j}} C_l D_l L_l \Bigg\} [1+o(1)] \quad . \tag{133}$$

A similar calculation gives

$$\text{imag}(h, \Upsilon^\epsilon h) = \min_{C_l} \max_{D_l} \sum_{j=1}^{N_r} \Bigg\{ \omega \sum_{l=1}^{n_{r_j}} \left(C_l^2 - D_l^2\right) L_l \\ -2 \sum_{\mathbf{x}_S \in \Omega_{r_j}} R(\mathbf{x}_S) f_R(\mathbf{x}_S) f_I(\mathbf{x}_S) \Bigg\} [1+o(1)] \quad . \tag{134}$$

We have thus shown that the complex map Υ^ϵ has a discrete approximation in the asymptotic limit $\epsilon \to 0$, that comes from the strong channeling of currents in the domain of the solution. The topology of the flow is strongly dependent on frequency. For low ω, current is essentially like the static one and is concentrated along paths of maximal conductivity. However, as ω increases, the topology of the flow can change dramatically because of the development of regions such as Ω_{c_j}, $j = 1, \ldots N_C$, that expell the electric and magnetic fields.

4.3 Discussion

The results of section 4.2 lead us to expect a network approximation of quasistatic transport in high contrast media. The topology of the network is clear at first, as explained above. However, the problem of associating to each branch in the network an impedance is more complicated. To understand the difficulty, consider the example in figure 10. The asymptotic approximation (133) is

$$-\text{real}(h, \Upsilon^\epsilon h) \approx R_1(C_1 - C_4)^2 - R_1(D_1 - D_4)^2 + R_2(C_1 - C_2)^2 \\ -R_2(D_1 - D_2)^2 + R_3(C_2 - C_3)^2 - R_3(D_2 - D_3)^2 \\ +R_4(C_3 - C_4)^2 - R_4(D_3 - D_4)^2 + 2\omega \sum_{l=1}^{4} C_l D_l L_l \quad , \tag{135}$$

and there is no min-max to take since all C_j and D_j, $j = 1, \ldots 4$, are fixed by the boundary conditions. In Ω we have strong currents concentrated along ridges of maximal σ that pass through the four saddle points and along the interface that surrounds the conducting region in the middle of the domain. Through the saddle points $1, 2, 3$ and 4 we have currents $(C_1 - C_4) + i(D_1 - D_4)$, $(C_2 - C_1) + i(D_2 - D_1)$, $(C_3 - C_2) + i(D_3 - D_2)$ and $(C_4 - C_3) + i(D_4 - D_3)$, respectively. Through the branches (e, h), (h, g), (g, f) and (f, e) we have counterclockwise currents $C_4 + iD_4$, $C_3 + iD_3$, $C_2 + iD_2$ and $C_1 + iD_1$, respectively. Thus, the conservation of current law (Kirchhoff's nodal law) is satisfied for arbitrary C_j and D_j, $j = 1, \ldots 4$. Nevertheless, in order to give to the approximation (135) a network interpretation, we must also have Kirchhoff's loop laws satisfied and they are not. Therefore we do not have a planar *network* approximation but

we do have a finite dimensional approximation for the boundary impedance operator Υ^ϵ. In general, the discrete approximation may or may not correspond to a unique planar network. The fact that we do not have a network is not, however, essential in inversion. What really counts is that the map Υ^ϵ has a unique, discrete asymptotic approximation, as given by (133) and (134). The asymptotic approximation of the magnetic field H and current $\nabla^\perp H$ in Ω are also uniquely determined, as explained in section 4.2. Finally, we have strong channeling of currents which means that boundary data available in inversion contain information about a few important features of the conductivity, such as saddle points and distribution of ridges of maximal σ in Ω. The issue of possible network forms of the discrete approximation of Υ^ϵ needs further study.

References

1. Allers, A., Santosa, F.: Stability and resolution analysis of a linearized problem in electrical impedance tomography, Inverse Problems **7** (1990) 515–533.
2. Alessandrini, G.: Stable determination of conductivity by boundary measurements, App. Anal. **27** (1988) 153–172.
3. Alumbaugh, D.L., Morrison, H. F.: Electromagnetic conductivity imaging with an iterative Born inversion, IEEE Transactions on Geosciences and Remote Sensing, **31** (1993) 758–763.
4. Alumbaugh, L., Morrison, H. F.: Monitoring subsurface changes over time with cross-well electromagnetic tomography, Geophysical Prospecting, **43** (1995) 873–902.
5. Bender, C. M., Orszag, S. A.: Advanced Mathematical Methods for Scientists and Engineers, McGraw-Hill, Inc., New York, 1978.
6. Berryman, J. G., Kohn, R. V.: Variational constraints for electrical impedance tomography, Phys. Rev. Lett. **65** (1990) 325–328.
7. Berryman, J. G.: Convexity properties of inverse problems with variational constraints, J. Franklin Inst. **328** (1991) 1–13.
8. Borcea, L.: Asymptotic Analysis of Quasistatic Transport in High Contrast Conductive Media, SIAM J. Appl. Math. **59** (1999) 597–639.
9. Borcea, L., Berryman, J. G., Papanicolaou, G. C.: High Contrast Impedance Tomography, Inverse Problems **12** (1996) 935–958.
10. Borcea, L., Berryman, J. G., Papanicolaou, G. C.: Matching pursuit for imaging high contrast conductive media, Inverse Problems **15** (1999) 811–849.
11. Borcea, L., Papanicolaou, G. C.: Network approximation for transport properties of high contrast materials, SIAM J. Appl. Math **58** (1998) 501–539.
12. Borcea L., Papanicolaou, G.C.: A Hybrid Numerical Method for High Contrast Conductivity Problems, Journal of Computational and Applied Mathematics **87** (1997) 61–78.
13. Calderón, A. P.: On an inverse boundary value problem, Seminar on Numerical Analysis and its Applications to Continuum Physics, Soc. Brasileira de Matematicá Rínftyo de Janeiro (1980) 65–73.
14. Cheney, M., Isaacson, D.: Distinguishability in impedance imaging, IEEE Trans. Biomed. Eng. **39** (1992) 852–860.
15. Cherkaeva, E., Tripp, A.: Inverse conductivity problem for noisy measurements, Inverse Problems **12** (1996) 869–883.

16. Cherkaev, A. V., Gibiansky, L. V.: Variational principles for complex conductivity, viscoelasticity, and similar problems in media with complex moduli, J. Math. Phys. **35** (1994) 127–145.
17. Courant, R., Hilbert, D.: Methods of Mathematical Physics, vol. I, Wiley, New York (1953) pp. 240–242 (Dirichlet's principle) and pp. 267–268 (Thomson's principle).
18. Curtis, E. B., Morrow, J. A.: Determining the resistors in a network, SIAM J. Appl. Math. **50** (1990) 918–930.
19. Curtis, E.B., Ingerman, D., Morrow, J. A.: Circular planar graphs and resistor networks, Linear Algebra Appl. 283 (1998) 115–150.
20. Dines, K. A., Lytle, R. J.: Analysis of electrical conductivity imaging, Geophysics **46** (1981) 1025–1036.
21. Dobson, D. C., Santosa, F.: Resolution and stability analysis of an inverse problem in electrical impedance tomography: dependence on the input current patterns, SIAM J. Appl. Math. **54** (1994) 1542–1560.
22. Fannjiang, A., Papanicolaou, G. C.: Convection enhanced diffusion for periodic flows, SIAM J. Appl. Math. 54 (1994) 333–408.
23. Fucks, L. F., Cheney, M., Isaacson, D., Gisser, D. G., Newell, J. C.: Detection and imaging of electric conductivity and permittivity at low frequency, IEEE Trans. Biomed. Eng. **38** (1991) 1106-1110.
24. Grünbaum, F. A., Zubelli, J. P.: Diffuse tomography: computational aspects of the isotropic case, Inverse Problems **8** (1992) 421–433.
25. Habashy, T. M., Groom, R. W., Spies, B. R.: Beyond the Born and Rytov approximations: nonlinear approach to electromagnetic scattering, Journal of Geophysical Research **98** (1993) 1759-1775.
26. Isaacson, D.: Distinguishability of conductivities by electric current computed tomography, IEEE Trans. Med. Imag. **MI-5** (1986) 91–95.
27. Isaacson, D., Cheney, D.: Current problems in impedance imaging, Inverse problems in partial differential equations, editors: Colton, D., Ewing, R., Rundell, W., SIAM (1990) 141–149.
28. Isakov, V.: Uniqueness and stability in multi-dimensional inverse problems, Inverse Problems **9** (1993) 579–621.
29. Isakov, V.: Inverse problems for partial differential equations, Springer-Verlag, New York (1998).
30. Ito, K., Kunisch, K.: The augmented Lagrangian method for parameter estimation in elliptic systems, SIAM J. Control and Optimization **28** (1990) 113–136.
31. Jackson, J. D.: Classical Electrodynamics, second ed., Wiley, New York (1974).
32. Kallman, J. S., Berryman, J. G.: Weighted least-squares methods for electrical impedance tomography, IEEE Trans. Med. Imaging **11** (1992) 284–292.
33. Keller, G. V.: Rock and Mineral Properties, Electromagnetic Methods in Applied Geophysics, Vol. 1, Theory, (ed. Nabighian, M. N.) (1988) 13–52.
34. Keller, J. B.: Conductivity of a Medium Containing a Dense Array of Perfectly Conducting Spheres or Cylinders or Nonconducting Cylinders, J. Appl. Phys. **34** (1963) 991-993.
35. Keller, J. B.: Effective conductivity of periodic composites composed of two very unequal conductors, J. Math. Phys. **28** (1987) 2516-2520.
36. Kevorkian, J., Cole, J. D.: Multiple scale and singular perturbation methods, Springer Verlag, New York (1996).
37. Kohn, R. V., McKenney, A.: Numerical implementation of a variational method for electrical impedance tomography, Inverse Problems **6** (1990) 389–414.
38. Kohn, R., Vogelius, M.: Determining conductivity by boundary measurements, Comm. Pure App. Math. **38** (1985) 643–667.

39. Kohn, R., Vogelius, M.: Relaxation of a variational method for impedance computed tomography, Comm. Pure Appl. Math. **40** (1987) 745–777.
40. Kozlov, S. M.: Geometric aspects of averaging, Russian Math. Surveys **44** (1989) 91–144.
41. Mallat, S., Zhang, Z.: Matching pursuit in a time-frequency dictionary, IEEE Trans. Signal Processing **41** (1993) 3397–3415.
42. Nachman, A. I.: Global uniqueness for a two-dimensional inverse boundary problem, Annals of Mathematics **142** (1995) 71–96.
43. Santosa, F., Vogelius, M.: A backprojection algorithm for electrical impedance imaging, SIAM J. Appl. Math. **50** (1990) 216–243.
44. Sylvester, J., Uhlmann, G.: A global uniqueness theorem for an inverse boundary value problem, Ann. Math. **125** (1987) 153–169.
45. Sylvester, J., Uhlmann, G.: The Dirichlet to Neumann map and applications, Inverse problems in partial differential equations, editors: Colton, D., Ewing, R., Rundell, W., SIAM (1990) 101–139.
46. Wexler, A., Fry, B., Neuman, M.: Impedance-computed tomography algorithm and system, Appl. Opt. **24** (1985) 3985–3982.
47. Yorkey, T. J., Webster, J. G., Tompkins, W. J.: Comparing reconstruction algorithms for electrical impedance tomography, IEEE Trans. Biomed. Eng. **BME-34** (1987) 843–852.
48. Zhou, Q., Becker, A., Morrison, H. F.: Audio-frequency electromagnetic tomography in 2-D, Geophysics (1993) 482–495.
49. Ziman, J. M.: Principles of the Theory of Solids, Cambridge University Press (1971).